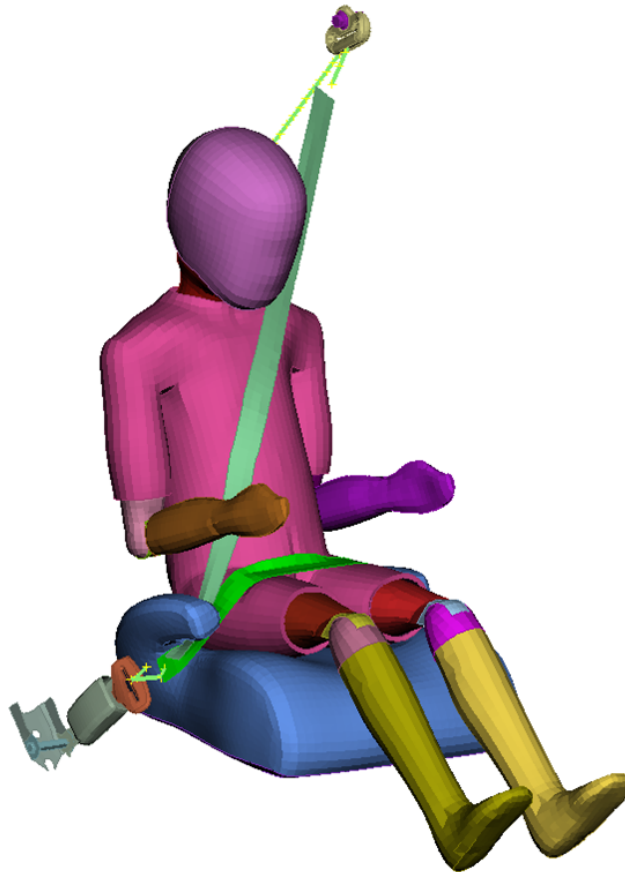# CHALMERS

Simulation and Analysis of Child Kinematics during Pre-Crash Maneuvers
FE-Simulation and Physical Testing
Master's thesis in Applied Mechanics and Automotive Engineering

EMELIE GUNTERBERG
ANNA JOHANSSON

Simulation and Analysis of Child Kinematics during Pre-Crash Maneuvers

FE-Simulation and Physical Testing

EMELIE GUNTERBERG
ANNA JOHANSSON

Cover:
The Q6 FE model seated on a booster cushion with a manually adjusted seatbelt.

Simulation and Analysis of Child Kinematics during
Pre-Crash Maneuvers
FE-Simulation and Physical Testing
Master's thesis in Applied Mechanics and Automotive Engineering

EMELIE GUNTERBERG
ANNA JOHANSSON
Department of Applied Mechanics
Division of Vehicle Safety
Chalmers University of Technology

ABSTRACT

Road traffic injuries are the most common cause of fatal injuries among children in the European Region (Sethi et al., 2008). Impacting the front passenger seat back is one of the main injury mechanism of AIS2+ head injuries for children aged 3-13 (Bohman et al., 2011a). Occupant and vehicle kinematics prior to and during a crash play an important role in the probability of the head impacting either the front seat or side door interior while seated in the rear seat. Studies also show that children who are placed on a belt positioning booster are less likely to sustain injuries than if only using a seat belt (Durbin et al., 2003). In a majority of cases with head contacts in frontal impacts, a steering or braking maneuver has preceeded the crash event in an attempt to avoid impact with the other vehicle or object (Bohman et al., 2011a). In order to understand the principals behind vehicle occupant injuries different anthropomorphic test devices (ATD) are available. The Q6 is an ATD representation of a six year old child available as both a physical dummy and as a finite element (FE) model. Little is known on its kinematics when influenced by low longitudinal and lateral accelerations as are present during a pre-crash maneuver. The purpose of this thesis was to investigate and compare the kinematics of the physical Q6 ATD (Q6 ATD) and the Q6 FE-model (Q6 model) placed on a booster in such maneuvers.

Physical tests were carried out comprising two turning maneuver tests (50km/h, 14m radius) and six emergency braking maneuver tests from 70km/h. During the braking maneuver test the Q6 ATD was positioned in three different positions; upright (T0), tilted 1 (T1) and tilted 2 (T2). Video images and vehicle data was used to analyze the head trajectories during the different maneuver tests.

The FE-simulations were carried out using FE models of a Volvo V60 vehicle body, rear seat, front seat and a model of a booster. The upright positioned Q6 model was simulated during a turning maneuver pulse similar to the physical turning maneuver test. It was also subjected to a braking maneuver pulse corresponding to the physical braking test. The same brake pulse was then used to carry out tests with the Q6 model seated in two different tilted positions, T1 and T2. In addition, two methods of pre-tensioning the belt was used for the FE-simulations.

The physical tests resulted in the turning maneuver causing the Q6 ATD to tilt sideways to a 14° angle. The braking maneuvers caused the Q6 ATD to have a forward forehead displacement of 115mm (T0), 130mm (T1) and 165mm (T2) respectively. The FE turning maneuver caused the Q6 model to tilt sideways to a 15° angle. The FE braking maneuver caused the Q6 model with a manual pretensioner to have a forward forehead displacement of 210mm (T0), 220mm (T1) and 220mm (T2). The FE braking maneuver using the automatic pretensioner caused the Q6 model's forehead to have a forward displacement of 230mm (T0), 185mm (T1) and 220mm (T2). During both the physical tests and the FE-simulations; the forward displacement increased with a larger tilting angle prior to braking.

The Q6 ATD and Q6 model showed similar behavior, as the tilting angle prior to braking had similar effects on the Q6 ATD and Q6 model. In pre-crash scenarios when turning occurs before braking, it is concluded that both the Q6 ATD's and the Q6 model's head has a greater longitudinal displacement with increasing tilting angle. This indicates that a combination of pre-crash maneuvers, may increase the risk of impacting the head.

While using the Q6 model for low pulse maneuvers has proven to be possible, it is important to keep in mind that both the Q6 ATD and Q6 model are designed for crash scenarios and are not validated for low pulse simulations. In order to use the Q6 ATD and Q6 model as a tool for evaluating child kinematics during pre-crash maneuvers comparisons with data from driving studies with real children need to be carried out.

Keywords: Q6, child safety, vehicle safety, pre-crash, kinematics, maneuvers

Preface

This Master of Science thesis project was initiated by the Safety Center (VCSC) at Volvo Car Corporation in collaboration with SAFER - Vehicle and Traffic Safety Centre at Chalmers University of Technology. The work was performed between January and June of 2012 at the department of Applied Mechanics, Vehicle Safety Division, for Volvo Cars. The examiner for this thesis was Adjunct Professor Lotta Jakobsson, Technical Leader at Volvo Cars.

We would like to thank Lotta Jakobsson and Anders Djärv (VCSC) for initiating this thesis. The selfless guidance and enthusiastic encouragement from our supervisors Isabelle Stockman, PhD Student (Chalmers University of Technology) and Tommy Spitza (VCSC) has been invaluable throughout this thesis work. The insights and support from Magnus Björklund (VCSC) as well as Lotta Jakobsson throughout the entire project are also immensely appreciated.

For the help in preparing the physical tests and the subsequent data extraction, Håkan Gustafsson and Jordanka Kovaceva at VCSC also deserve thankful recognition. For the ever so helpful support and nice chats in the coffee room we thank our co-workers at both Volvo Cars Safety Center and SAFER.

Nomenclature

AIS Abbreviated Injury Scale. A scaling system, established by the American Association for Medicine, used to define the severity of an injury (1 = minor, 6 = fatal) (Copes et al., 1989).

Animator Post processing program.

ANSA Pre processing program.

ATD Anthropomorphic Test Device and also called crash test dummies.

BC Booster cushion.

Cartesian coordinates Commonly used numerical coordinate system, were the axes meets in the origin (often 0,0,0 for three dimensional coordinate system) and two axes, making up a plane are perpendicular to the third axis and to each other.

CoG Center of Gravity.

Element Made up by nodes, for square linear shell elements, four nodes are needed.

FE Finite Element

H III Hybrid III, a family of ATDs.

LS-Dyna Finite Element Solver

Matlab Data extracting and programming program.

Mesh Consist of a number of elements, were the nodes are the calculation points.

MVC Motor vehicle crashes.

Node A point position in space, described with Cartesian coordinates

Out-of-design position A position of ATD that has not been intended and tested to have the wanted functions.

Pre-crash A maneuver that occurs prior to crash.

Primer Pre-processing program.

Pulse Describes the vehicles velocity and/or acceleration in Cartesian coordinates.

Q-series A family of ATDs.

Q6 An ATD representing a six-year old child.

Q6 ATD Refers to the physical Q6 used during physical testing at Stora Holm.

Q6 Model Refers to the simulation model representation of the Q6.

T0, T1, T2 Seating position in testing, zero tilted, medium tilted, and maximum tilted.

CONTENTS

1 Introduction

Road traffic injuries are the most common cause of fatal injuries among children in the European Region (Sethi et al., 2008). The leading cause of death among children aged 5-9 years in the United States in 2009 was unintentional violence where motor vehicle crashes (MVC) was the leading cause of violence (NCHS, 2012b). MVCs were next to cancer the single most common cause of child death in the United States in 2009 (NCHS, 2012a). In the European Union 16400 children under the age of 20 are killed every year by road traffic injuries, where at least one vehicle is present (Sethi et al., 2008). In addition, road traffic injuries are identified as the major cause of traumatic brain injuries leading to long-term disabilities among children in the European Region (Sethi et al., 2008). Results from analyses of child vehicle occupant fatalities show that more than 860 children aged 5-14 were killed in the United States in 2009 as a result of MVCs (NCHS, 2012b). In Sweden, during the late 1990's and early 2000's about 500-600 people were killed and 60 000-80 000 persons were injured every year as a result of road traffic accidents (Näringsdepartementet, 2004). The Swedish national approach to traffic safety was accepted by the government in 1997 and is summarized by the Vision Zero Initiative which states that "No loss of life is acceptable" (Trafikverket, 2012).

This thesis is part of an ongoing Ph.D. research project investigating the ability to replicate child passengers' kinematics in maneuver situations using ATDs. The Ph.D. project is in turn part of a larger research project aiming to further improve safety for children from 3 years old to small adults in the rear seat and is carried out at SAFER - Vehicle and Traffic Safety Centre at Chalmers (Jakobsson et al., 2011b).

1.1 Child Vehicle Safety

Belt positioning boosters reduce the risk of injuries for children (Arbogast et al. (2009), Jakobsson et al. (2005), Durbin et al. (2003)). Arbogast et al. (2009) show that children (aged 4-8) placed on belt positioning boosters were 45% less likely to sustain injuries than children of similar ages who were only using the seat belt. Durbin et al. (2003) also show that injuries to the abdomen and spine commonly associated with the seat belt syndrome were reduced when children were correctly placed on boosters with a proper belt fit in comparison to only utilizing a seat belt. Children up to about 10 years old do not have as well developed iliac spines of the pelvis as an adult (Burdi et al., 1969). The iliac spines play an important role in preventing the lap belt from sliding up on the abdomen and when these are lacking, a unique restraint solution is needed. For forward facing children seated on a belt positioning booster in the rear seat, the booster's guiding loops will help position the lap seat belt across the upper thighs rather than across the abdomen. In addition, a belt positioning booster will allow the child to have a comfortable leg position while sitting upright and thus preventing the child from slouching down (DeSantis et al., 1994). By using an age appropriate restraint system such as the booster for six year old children, the risk of obtaining either head or abdominal injuries is lowered (Wismans et al., 2008).

In order to prevent head injuries and mitigate severe consequences it is necessary to understand the injury mechanisms behind them. A study shows that the main injury mechanism of AIS2+ head injuries, for rear-seated children aged 3-13 restrained by a three point belt, is contact with the front passenger seat back, contact with side door interior or a non-contact rotational movement of the neck (Bohman et al., 2011a). The same study also identified an offset crash direction or vehicle maneuver as having an increasing impact on the presence of head injuries.

A driving study by Jakobsson et al. (2011a) shows that children aged 8-13 tilt laterally when driving in roundabouts or sharp turns. In addition, leaning in towards the middle of the vehicle was identified as a frequent behavior in order to have better visibility forward (Jakobsson et al., 2011a). During a lateral motion sequence, a study of kinematics and shoulder belt positions with children of ages 4-12 shows that the taller children in this range are more likely to raise the shoulder when subjected to lateral acceleration, thus preventing the shoulder belt to slip off. The shorter children showed no such effect and their movement caused by lateral acceleration can be described as a plain tilting motion of torso, thorax and head with pivot around the hips (Bohman et al., 2011b).

Studies have shown that the occupant trajectory due to pre-impact braking is much influenced by the foot location, and in particular the foot positioned most forward (Morris et al., 2005). This possibility of bracing the body is reduced for a normal 6 year old child as their stature would not allow them to reach the floor. Concerning pre-crash turning maneuvers the issues of passengers in the rear seat not having a steering wheel to hold on to may make them more easily influenced by lateral accelerations than an occupant in the drivers seat.

In addition the front seats often provide more side support than the rear seats, which also can mitigate lateral motion (Bose et al., 2008).

Occupant and vehicle kinematics prior to, and during, a crash play an important role in the probability of the head impacting either the front seat or side door interior while seated in the rear seat. The study conducted by Bohman et al. (2011a) shows that in a majority of cases with head contacts in frontal impacts, a steering or braking maneuver or a combination of both, has preceded the crash event in an attempt to avoid impact with the other vehicle or object. A previous study, conducted using a Hybrid III 6 year old physical ATD, has concluded the critical impact angle at which torso-roll out from the shoulder belt occurs to be 15° (Bidez et al., 2005). Both Bohman et al. (2011a) and Bidez et al. (2005) identify the torso as not being optimally restrained and that it is also subjected to rolling out of the seat belt due to an offset principal direction of force.

1.1.1 Available Test Tools

In order to obtain information about the cause of the injury mechanisms, crash data from real cases, physical ATD and mathematical models are often used. These are also valuable tools for further analyses and evaluation of the injury mechanisms.

The adult models of ATDs come in three sizes; 5th, 50th and 95th percentile representations. These sizes also come in different variations developed and validated for specific impact directions. Child ATDs come in different sizes depending on age. In Figure 1.1.1 children's body mass for 5th, 50th and 95th percentile children are represented for ranges between 0 to 20 year old. The variation of the mass of children grows bigger as they get older. For six year old children the variation in body mass between 5th, 50th and 95th percentile child is small. Therefore, the need to represent three child dummies of different sizes within each age group is not significant (Wismans et al., 2008). However, the need to represent children of different ages is of great importance as both the proportional size as well as strength between body parts vary a lot with age.
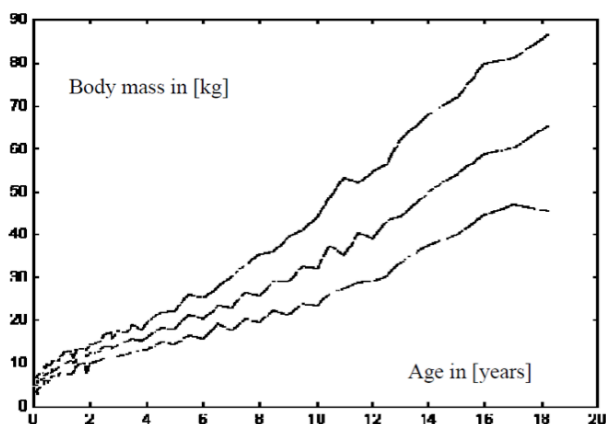

Figure 1.1.1: *Body mass of children of different ages, data collected over 18 years and from the US, Europe and Japan. It represents 5th, 50th and 95th percentile child body mass (Wismans et al., 2008).*

There are three families of ATDs representing children; HIII-, P- and Q-families. The HIII-family was developed in the United States and introduced to the US legislation at the end of the 1970s (Humanetics, 2010). The P-ATD family was developed in Europe during the 1970s and was initially designed to act as loading devices to be used during crash tests. The P-family had the correct geometry and mass distributions but had limited possibilities of measuring data. The P-dummies became approved in 1981 as the first European child ATDs (Wismans et al., 2008). In the 1990s the work with the P-family's successor, the Q-family, was initiated and is still under development. The Q-family has a more humanlike behavior than the P-family when comparing anthropometry, biomechanics, kinematics and injury risk assessment of critical parts of the body (Wismans et al., 2008). Existing data on children for development of ATDs is limited and much of the data used for child ATD development comes from cadaver tests on adults (Maurath, 2008). This data is then scaled down, which creates a problems since a child is not a scale factor of an adult (Maurath (2008), Burdi et al. (1969)). Figure 1.1.2 shows the proportional changes in the different body segments with increasing age emphasizing that biomechanical data from adults cannot replace data for children.

Physical ATDs are equipped with sensors which can measure forces and accelerations acting upon and within
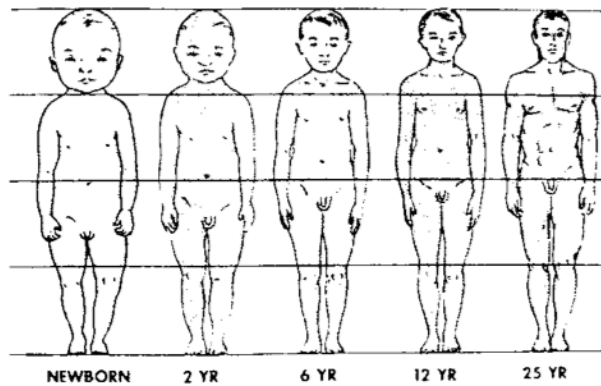
Figure 1.1.2: *Proportional changes in body segments with age (Burdi et al., 1969).*

the ATD during a crash. These measurements can then be used for interpretations of possible injuries that humans would have received during a crash of the same magnitude as tested. An ATD should be repeatable, reliable, anthropomorphic, biofidelic and have reproducible results (Maurath, 2008). A large part of the dummies are made of plastic materials, which means that they are naturally subjected to fatigue failure as a result from overloading. Plastic material is also known to get different material characteristics as they get older, they can dry out. These characteristics makes regular checks important to ensure performance consistency. The Q6-ATD's neck and lumbar spine is composed of metal and natural rubber, making it able to bend and shear in all directions. (Wismans et al., 2008). An aspect important to note is that the Q6 is made for frontal impacts and the Q6s is made for side impact. Neither are built for pre-crash scenarios, where the acceleration levels are lower than during a crash.

Mathematical simulations are becoming more important for developing crash safety and emphasizes that these models need to be adequate at emulating children (Johansson (2008), Maurath (2008)). An advantage of virtual testing is that it can be performed early in the design process, where no physical prototype need to exist, which saves both money and time (Maurath, 2008). The main advantage of using FE-models is their repeatability during testing. The tests and test set-ups can be saved and can therefore be performed over and over again, with the same or altered prerequisites. FE-models are often used when investigating new scenarios, as it is easier to alternate test setups as the development process evolves.

The FE-representation of the Q6 (v0.2) was released in 2011, making it a relatively new FE-model. An increasing number of consumer ratings are evaluating the safety performance of vehicle for rear occupants such as children. EuroNCAP is planning to use the Q6 in their dynamic assessment of Child Occupant Protection starting in 2015 (Lehmann, 2012). A status report by Wernicke et al. (2011) presented experiences with the Q6 physical and FE ATD and concluded that further detailed analysis of the Q6 under dynamic loading is necessary. They also concluded that due to lack of biomechanics-based injury criteria, only kinematics could currently be used during assessment of the Q6 in child restraint systems. An additional study comparing the physical ATDs Hybrid III 6yo and Q6 concluded that an introduction of the Q dummy in regulations and EuroNCAP might lead to unexpected effects such as the seat belt sliding up (Lubbe, 2010). Keeping these studies in mind, little is still known of the behavior of the Q6 physical and FE model and the area needs to be investigated further.

1.2 Purpose

The main objective of this thesis is to gain further knowledge about the kinematics of the Q6 ATD and Q6 model during events with low acceleration, also known as low pulse events. The low pulse events which are to be investigated in this thesis are braking and turning maneuvers. As of now, there are no ATDs and models especially designed for simulation of low-pulse scenarios, which is why an evaluation of the existing ATDs designed for crash pulses is valuable. The findings presented in this thesis will facilitate future work concerning the possibilities of using the Q6 ATD and Q6 model for low pulse simulations and their comparability to real children in low pulse events such as pre-crash maneuvers.

3

Research questions

- How similar are the kinematics of the Q6 model and the Q6 ATD?

- How does an evasive maneuver before crash affect the kinematics of the Q6 model during braking and/or during crash.

- How does a combination of evasive maneuvers affect kinematics in comparison to a single maneuver. I.e. the combined maneuver occurs in two steps; turning and then braking?

1.3 Limitations

Original FE-models of the vehicle body, vehicle rear- and front seats as well as a booster were used and provided by Volvo Cars. In addition the Q6 model (Humanetics) and belt retractor (Autoliv Inc.) were used. The scope of this thesis contains comparisons of kinematics between the Q6 model and the Q6 ATD. Validation of the Q6 model by comparison to real children, e.g. comparing biomechanical data was not taken into consideration.

2 Theory

In order to analyze the results of FE-simulations, some knowledge concerning the mathematical theory behind simulation programs is of great importance. In this chapter some mathematical theory together with some theoretical knowledge about the seat belt is presented.

2.1 Finite Element Method (FEM)

Finite element analysis can be divided into implicit and explicit methods. Normally, explicit method is used for fast simulation, when the system is time dependent. Furthermore, the implicit method is used for applications were stability is important (Ottosen et al., 1992). Newmark's method and the Newton Raphson Method are examples of commonly used implicit schemes. The implicit scheme is commonly used for static problems, where time-dependency can be neglected. As crash simulations are time dependent and dynamic simulations the implicit scheme is not appropriate as a solver, for these kinds of simulations. However, explicit calculations work well when the problem is time-dependent and dynamic. One negative aspect of the explicit approach is that the method can absorb energy from the system. It is also easy to misinterpret the results since the scheme can return non accurate results, rather than resulting in a failure to complete the simulations. Therefore it is important to know what to expect from the solution and to be able to analyze the results correctly. LS-Dyna is an FE application specialized in explicit scheme calculation and is therefore used extensively for crash simulations.

2.1.1 Seat belt

A modern standard 3-point seat belt comprises several parts, not just webbing, buckle, tongue and slip rings, see Figure 3.2.8. In order to allow some movement of the torso during travel the belt webbing is normally packed on a spring-loaded spool, also known as a retractor. This spool in turn is equipped with a locking device, which locks the webbing right above the spool when subjected to severe decelerations. This prevents the belt from feeding out during a crash or brake but allows for slow movements prior to and during travel, for example when buckling up. The locking device also eliminates any so-called film spool effect during a severe deceleration.

In addition a seat belt pretensioner is used to remove any belt slack by pulling the belt and giving it a tighter fit around the occupant's torso and lap in the event of a crash (*Automotive Handbook* 2011).

When simulating seat belt functions using FE-modeling it is important to note that pulling webbing (2D-elements) through a modeled slip ring is difficult and will result in many contact conflicts throughout the simulation. Therefore, the elements of the seat belt closest to the slip rings are commonly modeled with 1D-beam elements to eliminate this problem, Figure 2.1.1.
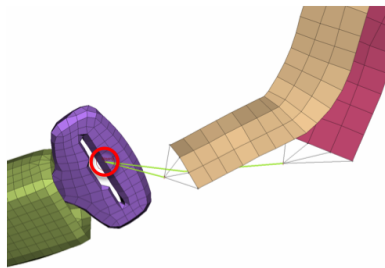

Figure 2.1.1: *Seat belt focusing on transition between the 2D and the 1D-elements which run through the slipring (red circle).*

The retractor and the pretensioner are usually time or displacement triggered when simulating. The time can be specified in a LS-Dyna trigger control card. The displacement is a maximum and a minimum distance allowed between two nodes (Hallquist, 2007). An example of how the pretensioner and retractor work is: in a crash simulation the pretensioner is triggered by an initial trigger time, releasing an original spring tensioner. This spring is represented by an LS-Dyna loading curve with displacement against force. The loading curve is triggered at a second trigger time, tightening the seat belt and locking it. As the crash event starts, forcing

the body to move forward more force is applied on the belt due to the locking device. A continued locking of the belt would result in the head continuing to move forward as the rest of the body is restrained by the seat belt. In order to mitigate the great forces and accelerations impacting the neck a load limiter is added. The load limiter allows the belt to be extended (at certain loads), and thereby decreases the relative acceleration between torso and head.

3 Method

Two methods were used in this study; physical testing and FE-simulations. Both methods included positioning the Q6 in the rear seat and performing turning and braking maneuvers. Different booster cushions (BCs), depicted in Figure 3.0.1, were used during the physical tests and FE-simulations. During the physical tests, a Britax Kid Plus with removed backrest was used. For measurements of the BCs see Appendix A.2. The main prerequisites of the physical testing and FE-simulations are shown in Table 3.0.1.

Figure 3.0.1: *The BCs used for physical testing at Stora Holm (Left) and for FE simulations (Right).*

Table 3.0.1: Major differences between physical test and FE-simulation

	Vehicle	BC	Seating Position	Turning Pulse
Physical Testing	XC70	Britax Kid Plus	Rear seat, right	Radius 14 m (Figure 3.1.2)
FE-Simulation	V60	Volvo In-house model	Rear seat, left	Radius 14 m

3.1 Physical Testing

Physical testing with turning and braking maneuvers were performed. In total two turning events were performed with the objective to analyze the Q6 ATDs kinematics due to lateral acceleration. A total of six braking events with different sitting postures were performed with the objective to analyze the forward displacements of the Q6 ATD.

3.1.1 Test Set-Up

The vehicle in use was a Volvo XC70, 2010 model year, driven by the same experienced test driver as in the studies by Bohman et al. (2011) and Stockman et al (2012). The vehicle data monitored included longitudinal and lateral acceleration, time, vehicle speed, yaw rate and brake pressure. During testing, the vehicle was equipped with 4 cameras where cameras 0 and 3 (Monacor TVCCD-30, lens focal length 3.6mm) captured a front view and lateral view respectively of the Q6 ATD. Camera 2 was positioned on the armrest in between the front seats in order to capture the side part of the BC to allow tracking of the lateral motion of the BC. Camera 1 captured a view of the outside environment from the front passenger seat window at a downward angle in order to identify the start and end cones of the track. The sample frequency of all cameras was 12,5 Hz.

The Q6 ATD was dressed with tight fitting cotton clothing in order to achieve similar friction between the belt and clothing as that of a child with a cotton t-shirt. The Q6 ATD was equipped with targets which were placed on key landmarks; shoulder lateral view, forehead front view, at the center of gravity of the head (CoG), thorax and jugular notch (Figure 3.1.1). The Q6 ATD was placed in the rightmost rear seat on a BC, seen in Figure 3.0.1.

The track used for the turning maneuver was a quarter of a circle track with a radius of 14 meters, see Figure 3.1.2. Cones 1 and 2 advised the driver where to start and stop the turning procedure. In addition the cones allowed the camera placed inside the vehicle to identify when in time the vehicle entered and exited the track. The braking test was carried out along the straight track number 3 (Figure 3.1.2), where the maximum capacity braking was initiated at cone 1 (Figure 3.1.2).

Figure 3.1.1: *The Q6 ATD in its initial positions with targets on key landmarks marked in vehicle and on Q6 ATD. TL: Front view tilted 0. TR: Front view tilted 1. BL: Side view tilted 0. BR: Front view tilted 2*
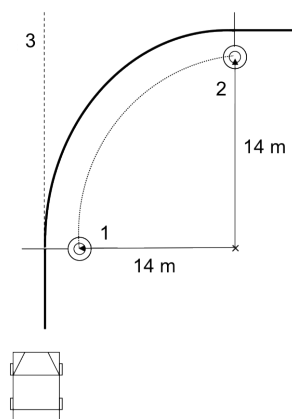

Figure 3.1.2: *Schematic view of test track. Turning track along continuos line and braking maneuvers along dashed line.*

3.1.2 Physical Test Procedure

During all tests, data was recorded in the vehicle during the time the engine was running. During test runs 1-4, Table 3.1.1, the Q6 ATD was placed in a fully upright position where the Q6 ATD's hips, thighs and lower back was pushed firmly into the BC as well as rearwards into the vehicle's rear seat back. The Q6 ATD was belted with the standard seat belt where the lap was fed under the guiding loops and the shoulder belt fed under the left guiding loop of the BC. The shoulder belt was tightened by pulling the upper part allowing the belt to position itself across the thorax and over the clavicle. No subsequent shoulder belt position adjustment was made. For the breaking tests the average longitudinal deceleration was 8.4 m/s^2 and for the turning tests the average lateral acceleration was 7.9 m/s^2. During tests 5 and 6 the Q6 ATD was tilted at an initial angle of 7°

Table 3.1.1: Executed physical test runs with the Q6 ATD at Stora Holm.

Test Run (TR-Ph)	Maneuver	Sitting Position	Longitudinal Initial Speed [km/h]	Longitudinal Avg Acc [m/s^2]	Lateral Avg Acc [m/s^2]	Initial Tilt Angle [deg]
1	Brake	Tilted 0 (T0)	67	-8.3	-	0
2	Brake	Tilted 0 (T0)	67	-8.1	-	0
3	Turn	Tilted 0 (T0)	47	-	7.8	0
4	Turn	Tilted 0 (T0)	47	-	8.0	0
5	Brake	Tilted 1 (T1)	66	-8.2	-	7
6	Brake	Tilted 1 (T1)	67	-8.5	-	6
7	Brake	Tilted 2 (T2)	67	-8.3	-	11
8	Brake	Tilted 2 (T2)	70	-9.0	-	12

and 6° respectively. These tilting angles correspond to the shoulder belt's outermost edge being positioned in line with the outermost part of the shoulder, see Figure 3.1.1. During tests 7 and 8 the Q6 ATD was positioned at angle of 11° and 12° respectively, corresponding to the innermost edge of the shoulder belt being in line with the outmost part of the shoulder.

Turning maneuver

During the two turning maneuver tests the vehicle started the turning maneuver when passing traffic cone 1 and followed the curve until cone 2, see Figure 3.1.2.The average longitudinal speed, at cone 1 for the two turning test runs was 47 km/h. The average longitudinal speed through the entire curve of the two turning test runs was 43 km/h. The average lateral acceleration through the entire curve of the two turning test runs was 7.9 m/s^2 (Table 3.1.1).

There was no possibility of real-time video extraction at the test track which would have been beneficial in order to obtain the maximum tilting angle of the Q6 ATD during the turning tests to be used during the braking tests. Therefore the maximum tilting angle was estimated in order to position the Q6 ATD for the succeeding braking tests. The initial tilting angles were measured just before the turning event (at cone 1) and the error with respect to the initial positioning was ∼1% between the two turning test runs. This error is due to vehicle acceleration on the track in order to achieve the correct initial speed prior to maneuvering.

The vehicle's position was calculated when the Q6 ATD had tilted to the angles represented by T1 and T2 during the curve. The distance travelled by the vehicle was calculated by assuming a perfect curve, constant radius, based on the average lateral acceleration and the average longitudinal speed throughout the curve. The initial ramping of the acceleration was not taken into account during these calculations and the vehicle was assumed to start turning in an instant.

Braking maneuver

During the 6 braking tests the vehicle was braked with maximal capacity to a full stop starting at cone 1 (Figure 3.1.2). The initial average longitudinal speed of the four runs was 67 km/h at cone 1 where the driver braked with maximum capacity to a complete stop, see Table 3.1.1. The average deceleration, observed without the ramping, was 8.4 m/s^2 (Table 3.1.1).

3.1.3 Method of Analysis

In order to identify the turning and braking events, the data and video were viewed simultaneously. The software TEMA v3.12 (Image Systems) was used in order to track the images collected from both the frontal and lateral cameras. MATLAB v.R2012a (MathWorks) was used to process all other data from the physical testing. Relevant image frames for the turning maneuver were extracted, starting at the time index closest to when the lateral acceleration was equal to 0.25m/s^2. The last time index was set to when the Q6 ATD's head had reached maximum positive lateral movement. For the braking maneuvers, the relevant image frames were collected starting at the final time index prior to the brake pressure changing from zero to a positive value. The last time index was set by visually monitoring when the Q6 ATD's head returned to rest on the rear seat back.

The front view was used to track the lateral and vertical displacement of the forehead as well as the tilting angle of the torso during turning maneuvers. The side view was used to track longitudinal and vertical movement of the forehead as well as the head's CoG on the side of the ATDs head, Figure 3.1.1.

One input parameter needed for correct tracking of images in TEMA is the distance between the camera plane and the target. As the Q6 ATD had three different initial tilting angles for the braking test runs, the distance from the camera plane at the lateral camera and the Q6 ATD's XZ plane varied both between the different test runs as well as within each test run. For each braking test run, an average lateral displacement of the head was obtained through tracking via the front view camera. The average displacement was considered a sufficient measure, as the maximum difference of lateral displacements within each braking test run was 40mm. This lateral difference of 40 mm contributed to a longitudinal displacement of 7mm during tracking, which was considered trivial. When tracking the front view for the turning test runs the Q6 ATD moved within its initial YZ plane. Therefore it was not needed to alter the distance between the camera plane and target.

When analyzing the tilting angles from the front view, the vertical line passing through the center of the headrest and the Q6 ATD center sagittal plane for the "Tilted 0" position (Figure 3.1.1) was set as 0 degrees. Tilting angles inwards the vehicle have negative values in accordance with the global vehicle coordinate system, see Figure 3.1.3. The vehicle data from the braking tests was extracted and analyzed, showing that the test runs had good repeatability, see Figure 3.2.4.
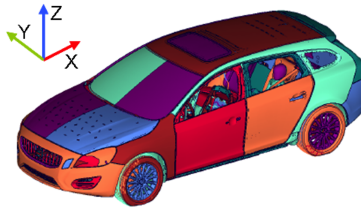

Figure 3.1.3: *The vehicle coordinate system depicted using a Volvo V60 FE-model. X-Longitudinal, Y-Lateral and Z-Vertical.*

3.2 FE simulations

The simulation procedure of the Q6 model in pre-crash maneuvers was made in steps as seen in Figure 3.2.1. The main steps were preparation of V60 sled; squashing of rear seat and BC, pulse preparation, positioning of Q6 model, seat belt modelling and finally the pretensioner and retractor was modified. After each step results were analyzed and if needed returned to a previous step. Data extraction and plotting of curves has been executed using the software MATLAB v.R2012a (MathWorks) and the Post-Processor Animator4 v.18254 (Gesellschaft fur numerische Simulation, GNS). The pre-processors used were ANSA v.13.2.2 (NVIDIA Corporation) and PRIMER v.10.1 (Oasys Ltd).

3.2.1 Rear seat and BC

In order to position the Q6 model on the BC (Figure 3.0.1), the BC needed to be pressed down into the rear seat in order to avoid element interlocking due to contact failure and to get in the right position. When pressing the Q6 model to its desired final position prior to simulation the rear seat and BC's elements were deformed as shown in Figure 3.2.2.
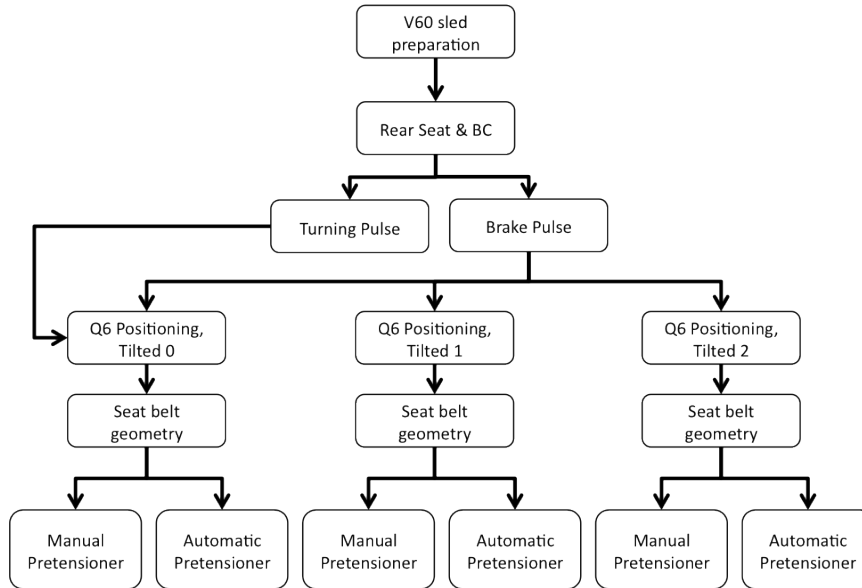
Figure 3.2.1: *Flow chart showing the different simulation steps and components used.*
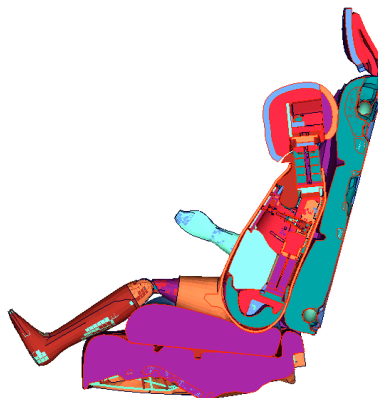

Figure 3.2.2: *Cross section of squashed rear seat and squashed BC depicting the initial penetration depth.*

3.2.2 Vehicle Movement

Pulses were made for braking and turning maneuvers based on the physical tests at Stora Holm, see Figure 3.2.3 and Figure 3.2.4. The pulse was added to a rigid bottom plate connected to rigid parts at the front and rear part of the sled. These rigid parts constrain the car, transforming the pulse upon the whole structure. The turning pulse was created to represent a 90° turn along a 14 meter radius track with a speed of 50 km/h, leading to a lateral acceleration of $13.8 m/s^2$. The corresponding X, Y, Z translational velocities (Figure 3.2.3) and X, Y, Z rotational velocities were calculated and processed for simulation format. The vehicle was set to a constant velocity of 50km/h for 180ms prior to turning. No ramping of the acceleration was taken into account, thus the vehicle was assumed to start turning in an instant. The decelerations of the vehicle during
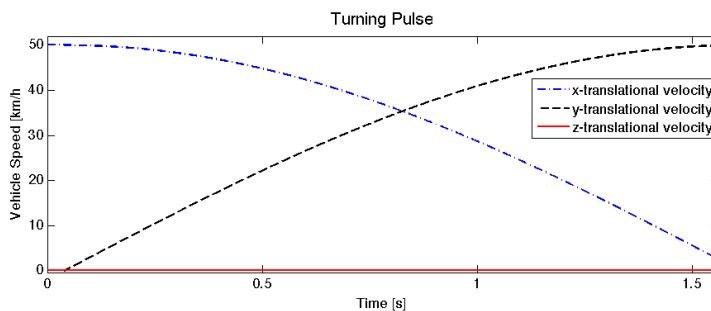
Figure 3.2.3: *X, Y and Z velocity during turning maneuver for TR-Ph 3 and 4.*

the physical tests was analyzed. The average decelerations of TR-Ph 1,2 and 5-8 were extracted and linearized, Figure 3.2.4. The coefficient of determination, R^2, for the linear regression equaled 0,91 which was considered sufficient. As shown in Figure 3.2.4 the linearized curve was set to start at 70km/h with a constant velocity during the first 300ms.
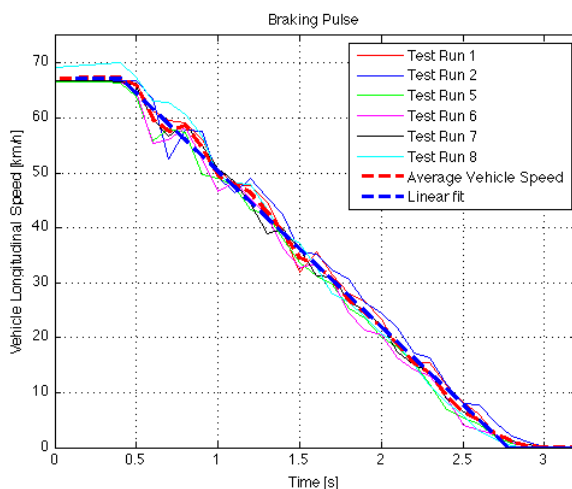
Figure 3.2.4: *Longitudinal velocity of TR-Ph 1,2,5-8 and linear fit for FE-braking pulse preparation*

3.2.3 Q6 Model

The FE-simulations were carried out using the Q6 model in its original status (Humanetics, 2010). No adjustments have been made regarding material data, functions or meshing. The Q6 model joints have however been adjusted in order to allow positioning in the vehicle environment.

The Q6 model is made up of many different parts. One feature is that it has an outer layer of solid elements and one layer of shell elements, creating a suit which covers the torso, half of the thighs and arms, Figure 3.2.5. Due to this suit, rotation of the hip region needed to be simulated, in order to get the correct sitting posture for the V60 rear seat. The default hip angle for the Q6 model is 90°, which then has been increased by 10° by

performing a pre-simulation. Since the arms and knees were not surrounded by this suit, it was possible to rotate these joints without carrying out any pre-simulations. After placing the Q6 model and BC in the center
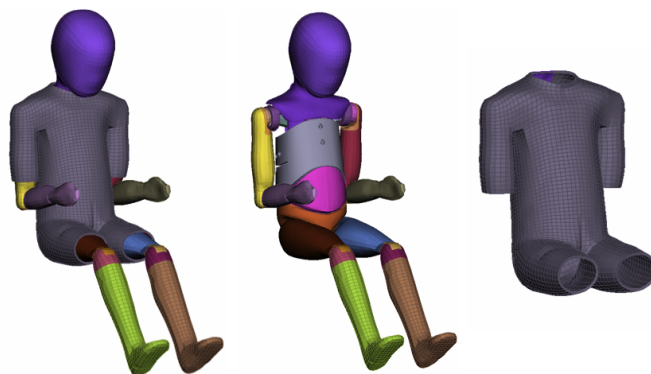

Figure 3.2.5: *Q6 model in three views, from the left; The whole Q6 model, the model without the suit and the suit consisting of one layer of solid elements and one layer of shell elements.*

of the rear left seat, the Q6 model was tilted to two different angles, T1 and T2. The final tilting position for automatic pretensioner and manual pretensioner at time zero for braking pulse are seen in Figure 3.2.6 and Figure 3.2.7. The tilting angles were aiming to represent the different tilting angles observed and measured
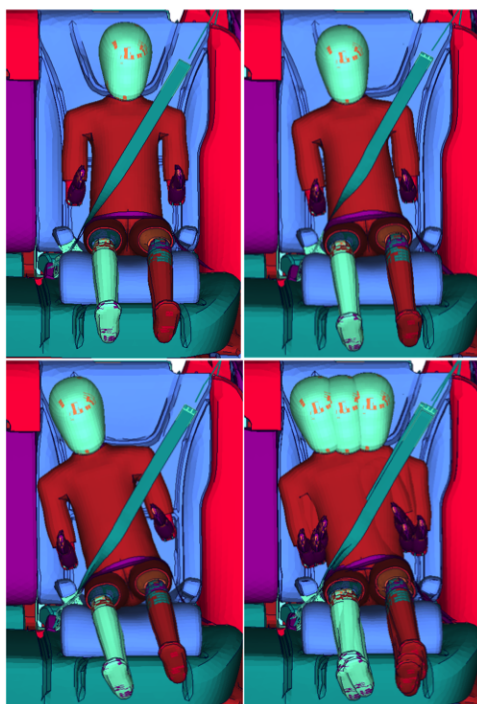
Figure 3.2.6: *The tilted Q6 model for automatic pretensioner, at time zero. TL: T0. TR: T1. BL: T2. BR: T1,2,3 in one frame.*

during the physical testing. The Q6 model was only tilted once for each tilting angle, with PRIMER, however, the belt geometry varies due to pre-simulation of the manual pretensioner described in Section 3.2.4.

3.2.4   Seat Belt Geometry

The seat belt's initial geometry was built using the ANSA seat belt tool, Figure 3.2.8. The issue of guiding the seat belt under the BC's guiding loops is not accounted for in ANSAs automatic seat belt tool. The tool allows for a connecting A-B functionality and wrapping around the Q6 model which is sufficient for models positioned
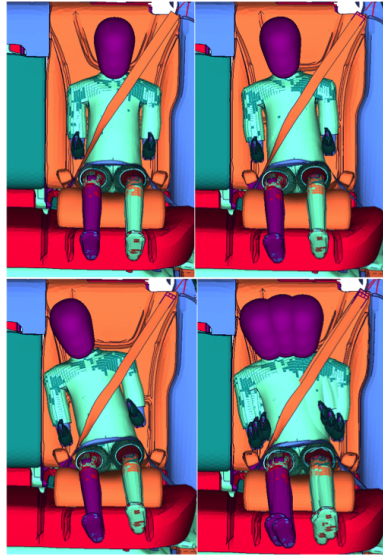
Figure 3.2.7: *The tilted Q6 model for manual pretensioner, at time zero. TL: T0. TR: T1. BL: T2. BR: T1,2,3 in one frame*

directly on the rear seat. However, the presence of a BC resulted in a need for manually adjusting the seat belt to a large degree. The 2D-element parts of the shoulder and lap belt were set to three elements wide with an element size of 12x12 mm. In the lower regions where the belt passed the guiding loops, beam elements with no mass (zero beam elements) were added and placed on both the BC and along the belts edges, Figure 3.2.9. These zero beam elements together with an LS-Dyna edge-to-edge contact served to prevent penetration of the BC with the 2D part of the seat belt. In addition, the element size of the 2D belt in this region was decreased to lower the possibility of penetration.
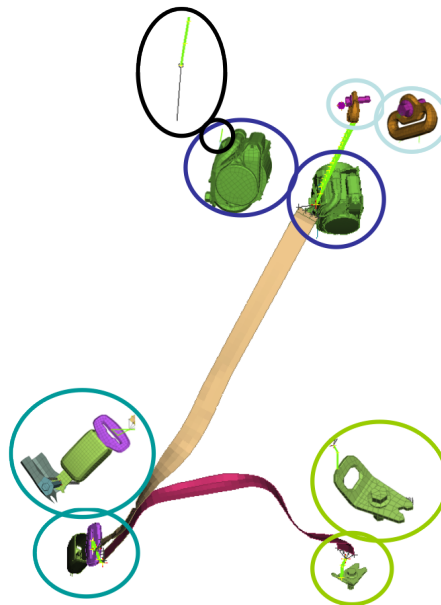
Figure 3.2.8: *TL: Joint between belt elements and retractor. TR: Upper webbing slip ring guide with attachment to chassis. BL: Belt buckle and tongue attached to chassis. BR: Lower belt attachment to chassis*

When modeling the seat belt for the different tilting angles, the upper and lower parts of the T0 seat belt were saved and reused when modeling T1 and T2. This saved modeling time and allowed the angle at which the belt approached the Q6 model from the upper webbing attachment to stay the same through all tilting angles of the Q6 model. The output from ANSA's automatic seat belt tool, with performed adjustments is
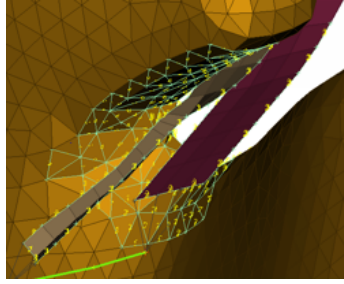
Figure 3.2.9: *Added beam elements to avoid unwanted penetration, the beams were added in the guiding loops and around the belt element nearby.*

seen in Figure 3.2.10. This seat belt was used during automatic pretensioner simulations. The original seat belt position was the one used for the pre-simulation for the manual pretensioner, where a boundary prescribed motion was added as described below.
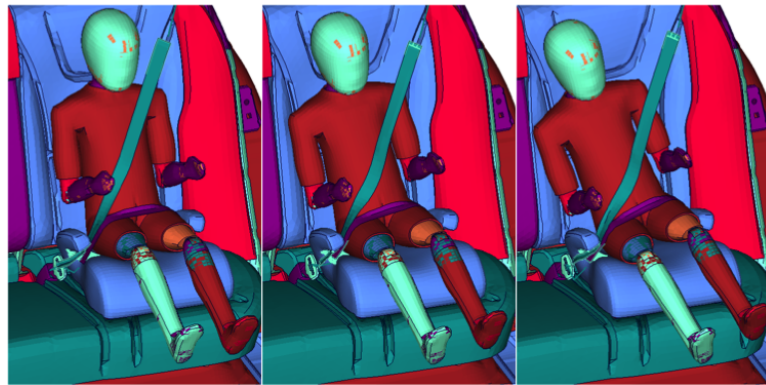

Figure 3.2.10: *The original belt position after using ANSA's automatic seat belt tool with adjustments. From the left: T0, T1 and T2.*

Retractor and Pretensioner

In order to remove seat belt slack, two different methods of pre-tensioning were used. The first method was based on manually pulling the belt prior to final simulation. This was executed by adding a boundary prescribed motion to the final node of the shoulder belt connected to the retractor. It was set to 140mm in a pure negative Z direction, see top left in Figure 3.2.8. This value was set as a trade-off between having to create a tight fit but not wanting to much distortion of the Q6 model's elements. The simulation was run with the original pretensioner turned off, and the trigger times for all retractor parts were set to 0. Later, the new positions of all nodes (Q6 model, seat, BC, belt, sled) were saved. The belt, which now had a tight fit over torso and lap, then had to be manually adjusted further in order to thread it under the guiding loops.

The second method included using a version of the retractor with a modified automatic pretensioner. This pretensioner is in reality used to remove slack during a crash and therefore needs to function fast and with high force. The purpose of the pretensioner in this thesis was merely to tighten the belt prior to braking and therefore these values were decreased. The original and adjusted values are listed in Table 3.2.1.

In the braking simulation the vehicle drove for 300ms before the braking maneuver started in order to allow the Q6 model to settle. This time, 300ms, is defined as the time prior to braking. During the automatic pretensioner simulations, the seat belt positions prior to braking looked as depicted in Figure 3.2.11. Here the seat belt positions varied between the different tilting angles. For T0, left in Figure 3.2.11 the shoulder belt experienced a lot of slack and its 1D elements penetrated the BC. For T1, middle picture, however, the shoulder-belt still passed the guiding loops, leading to less belt slack. In T2, the shoulder belt experienced slack as well as penetration of 1D elements in the BC, similar to T0. The manual pretensioner pre-simulations were set to last for 100ms. The resulting belt positions after this manual pre-simulation are seen in Figure 3.2.12. The 2D part of the seat belt was higher up on the abdomen, then in the original position prior to pre-simulation.

Table 3.2.1: Displacement and force curves for the pretensioner.

Original		Adjusted	
Displacement/Rotation mm/rad	Force/Moment 1/mm	Displacement/Rotation mm/rad	Force/Moment 1/mm
200	2	180	0.2
59.9999	1.8	150	0.18
0.0	0.01	120	0.16
-100.0	-10.00	100	0.14
		80	0.12
		60	0.10
		40	0.08
		20	0.06
		0.0	0.04
		-100.0	-10.0
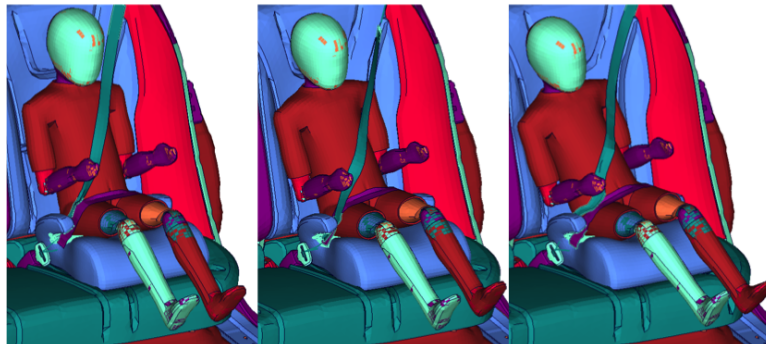
Figure 3.2.11: *Belt position prior to braking, from left: T0, T1 and T2.*

Further, the 1D elements at the lower shoulder belt penetrated the BC. Adjustments were made so that the seat belt looked like in Figure 3.2.13, these seat belts had minimized slack and the 2D elements passed the guiding loops. For the manual pretensioner braking pulse, the pretensioner was turned of by setting the trigger time to
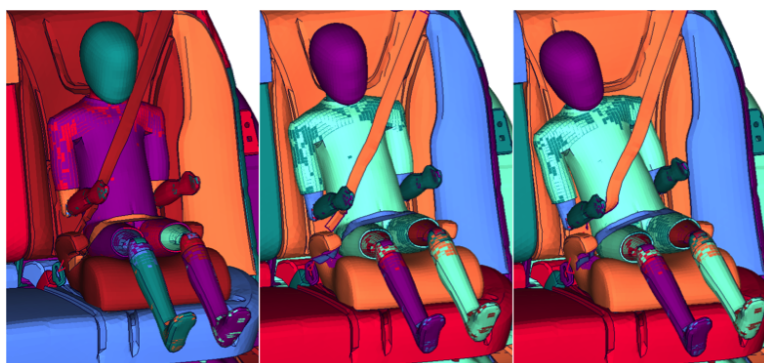
Figure 3.2.12: *Belt position after manual pretensioner simulation but and before adjustments were made.*

zero for the pretensioner. Belt positions prior to braking for the manual pretensioner are seen in Figure 3.2.13, which showed less variation in seat belt position prior to braking than seen for automatic pretensioner in Figure 3.2.11.
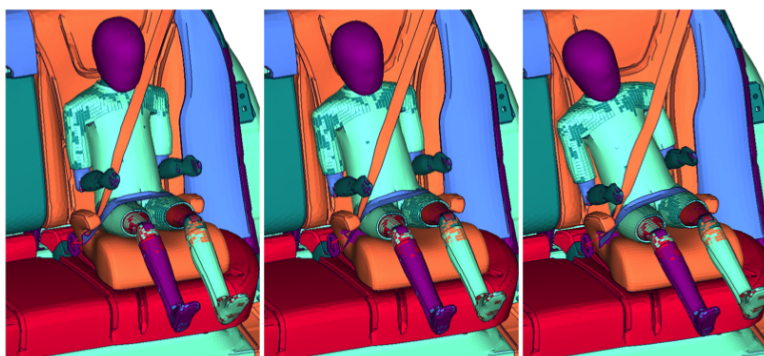
Figure 3.2.13: *Manual pretension position prior to braking, identical to the initial position in the braking pulse, no pretensioner activated here. The manual pretensioner was done in a pre-simulation.*

3.2.5 FE Test Procedure

In total nine simulations were run on pre-crash maneuvers. During TR-FE1-4, the manual pretensioner was used and for TR-FE5-8 the automatic pretensioner was used, as seen in Table 3.2.2. For TR-FE 9 an automatic pretensioner was used, but it was not pulling the belt upwards. Also the friction between BC and rear seat was lower for this run, 0.5 compared to the increased value of 0.8 for the other test runs. For all simulations performed, specifications like material data and hourglassing were used unchanged from the original model. Some specifications like contacts and friction files were altered to fit our simulations. How they were altered and some adjusted include files are found in Appendix B.

The vehicle's position was calculated when the Q6 model had tilted to the angles represented by T1 and T2 during the curve. The radius and longitudinal speed was known and constant, hence the lateral acceleration was calculated to 13.8 m/s^2.

3.2.6 Method of analysis

In order to calculate angles due to turning maneuvers as well as the initial tilting angles the same nodes on the Q6 model were used through all test runs, see Figure 3.2.14. The tilting angle of the head was calculated between a node on the center of the forehead (N3) and a node on the lower abdomen (N1). The tilting angle of

Table 3.2.2: Executed FE test runs with the Q6 model. *non functional automatic pretensioner and lower friction between BC and rear seat.

Test Run FE (TR-FE)	Maneuver	Sitting Position	Pretensioner	Initial Tilt Angle Prior to braking [deg]
1	Brake	Tilted 0 (T0)	Manual	0
2	Brake	Tilted 1 (T1)	Manual	5.7
3	Brake	Tilted 2 (T2)	Manual	15
4	Turn	Tilted 0 (T0)	Manual	-
5	Brake	Tilted 0 (T0)	Automatic	0
6	Brake	Tilted 1 (T1)	Automatic	5.8
7	Brake	Tilted 2 (T2)	Automatic	13
8	Turn	Tilted 0 (T0)	Automatic	-
9	Brake	Tilted 0 (T0)	Automatic*	0

the torso used the same lower abdomen node (N1) together with a reference node placed close to the jugular notch (N2).

To get the X and Z displacements in the braking maneuvers, the center node of the forehead was chosen. For the X and Z displacements with respect to the head's CoG, a node on the side of the Q6 model's head was chosen. Due to the same node numbers in all simulations, the same point could be used for all simulations. Data from the simulation with all these nodes were extracted with respect to time using ANIMATOR and plotted using Matlab.
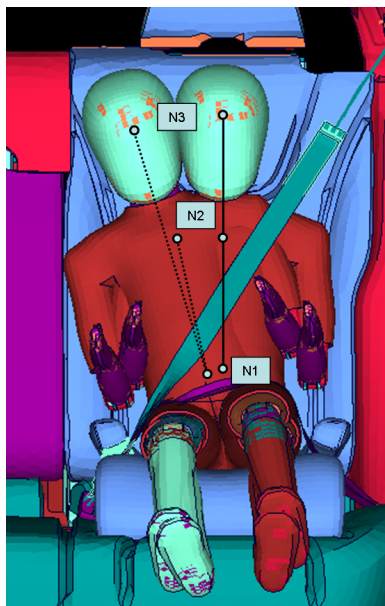
Figure 3.2.14: *Schematic location of nodes (N1, N2, N3) used for measuring tilting angles due to braking and initial positioning.*

4 Results

The results are divided into Physical testing, FE- modeling and their correlation to each other.

4.1 Physical Testing

In Figure 4.1.1 and Figure 4.1.2 the X and Z displacements of the forehead and CoG are shown from the physical testing with the Q6 ATD during braking. In these figures the longitudinal and vertical displacements (X,Z) are all set to start in a (X,Z)=(0,0) position. Figure 4.1.1 show that TR-Ph 1 and TR-Ph 2, where the Q6 ATD was positioned in an upright position, resulted in a smaller forward (X) displacement than TR-Ph 5-TR-Ph 8. The test runs were the Q6 ATD was in a T1 position generally resulted in a smaller forward displacement than the results from the T2 positions which indicated the largest forward displacement of all.
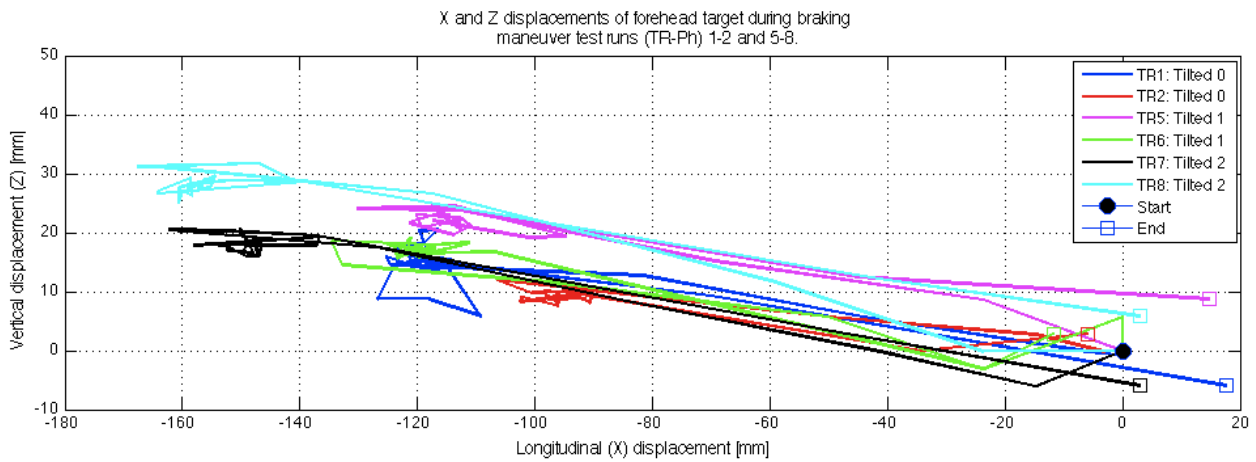
Figure 4.1.1: *X and Z displacement of forehead during braking test runs*
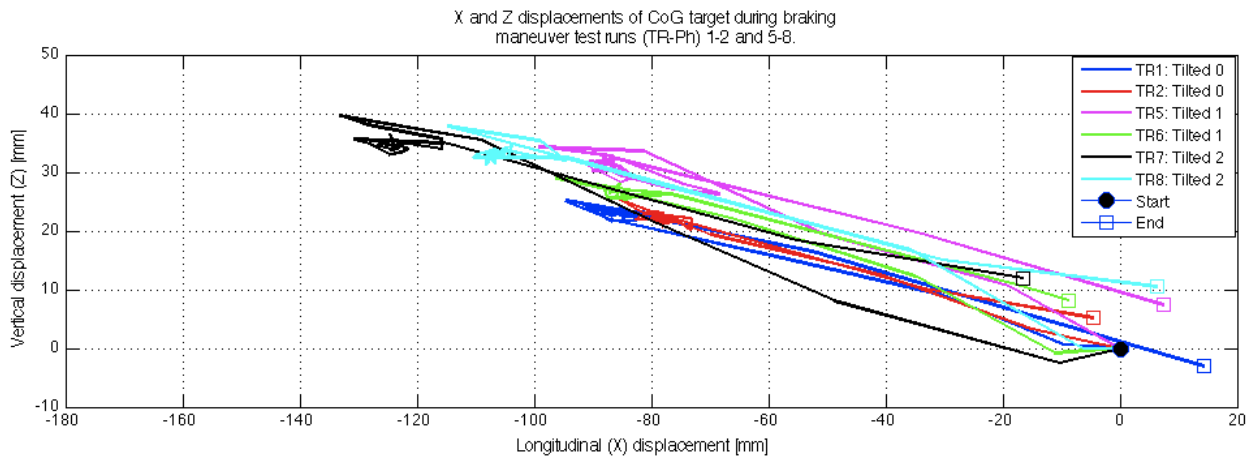
Figure 4.1.2: *X and Z displacement of the head's CoG during braking test runs*

In Table 4.1.1 the average maximum forward displacements are displayed for the different test positions. The maximum difference in forward displacement of the forehead was 60 mm, generated by subtracting TR-Ph 8 and TR-Ph 2. The maximum difference in forward displacement of the head's CoG is 45 mm generated by subtracting TR-Ph 7 and TR-Ph 2. Further results from the physical tests are found in Appendix A, Table A.1.1.

The distance traveled calculated as described in Section 3.1.2 are seen in Table 4.1.2. In Table 4.1.2 the

Table 4.1.1: Average values of the forward displacements and tilting angles for the physical testing.

Test Runs Physical	Avg Max Displacement Forehead [mm]	Avg Max Displacement Head CoG [mm]	Max Tilting Angle [deg]	Initial Tilting Angle [deg]
TR-Ph 1,2	115	90	-	0
TR-Ph 3,4	-	-	14	0
TR-Ph 5,6	130	100	7	7
TR-Ph 7,8	165	125	12	12

distance traveled for the vehicle during the physical tests are presented with the corresponding tilting angles of the Q6 ATD. As the physical data is sampled at 80ms the exact angles corresponding to the maximum tilting angles of the FE-simulation cannot be extracted, see Table 4.2.1. To achieve the tilting angles of 13.3° (~T2) and 15° (max tilt angle) during the physical turn maneuver, the vehicle needed to travel 23m and 25m along the calculated curve with constant radius as described in Section 3.2.2. The vehicle would also need to have had a Y translation of 12.5m and 14.5m respectively to reach the T2 tilting angles of Table 4.2.1. In order to achieve tilting angles of 5.1° and 11°, the physical vehicle needed to travel 4 m and 6.5m respectively. The corresponding Y translation of the vehicle was 0.4m and 1m.

Table 4.1.2: The physical vehicle's position along the test track relative to the Q6 ATD's tilting angle during the turning maneuver.

Tilt angle [deg]	Time elapsed [ms]	Distance traveled [m]	X translation [m]	Y translation [m]
5.1	320	4	4	0.5
11	560	6.5	6.5	1
13.3	1920	23	17	12.5
15	2080	25	17.5	14.5

4.2   FE Simulation

Braking and turning maneuvers in FE simulations were divided into usage of automatic pretensioner and manual pretensioner, see Figure 3.2.1.

4.2.1   Manual pretensioner

For the manual pretensioner T2 showed a greater X and Z displacement for the head's CoG than T1 and T0, as seen in Figure 4.2.1. It can also be seen that T1 had greater X and Z displacements of the head's CoG than T0. T2 also had greater X and Z displacements for the forehead compared to T1 and T0, Figure 4.2.2. T0 had the smallest X and Z displacements. The maximum forward displacements of the Q6 model in braking maneuvers for manual pretensioner is shown in Figure 4.2.3. The forward displacements from the simulations were extracted between 0-1000 ms of the simulation time, not the full curve which lasted until 1560ms.

4.2.2   Automatic pretensioner

For the automatic pretensioner the head's CoG X and Z displacements are seen in figure Figure 4.2.4. T0 showed the highest forward displacement and T1 the lowest. In Figure 4.2.5 the forehead X and Z displacement are seen. Similar to the head's CoG, the forward displacement of the forehead was greatest in T0 whereas T1 had the lowest.

The lower friction in TR-FE 9 made the Q6 model slide together with the BC on the rear seat rather than the Q6 model sliding on top of the BC. For further friction data on the simulations see Appendix B. The X and Z displacement for the head's CoG and forehead for the low friction scenario is shown in Figure 4.2.6 and in Figure 4.2.7 respectively.
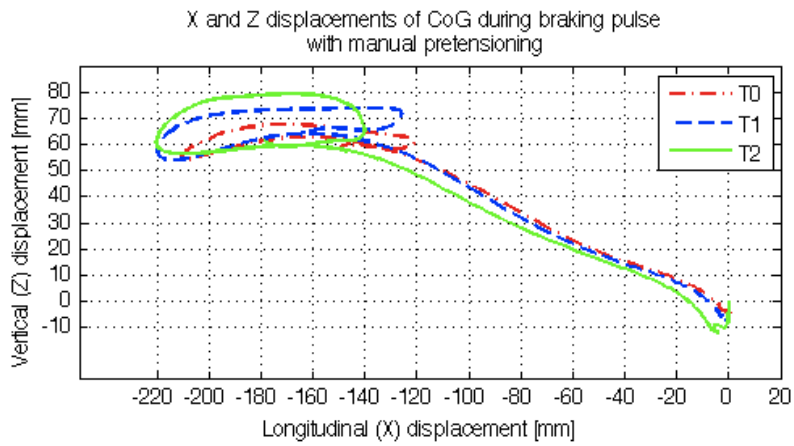
Figure 4.2.1: *X and Z displacement of CoG during braking test runs with manual pretensioning*
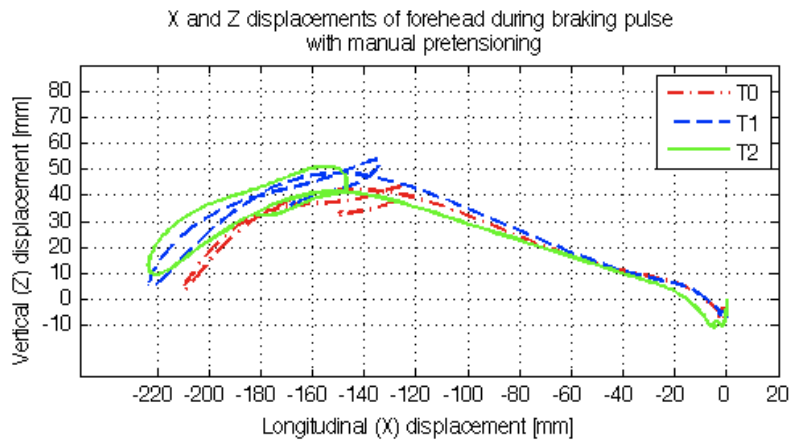

Figure 4.2.2: *X and Z displacement of forehead during braking test runs with manual pretensioning*
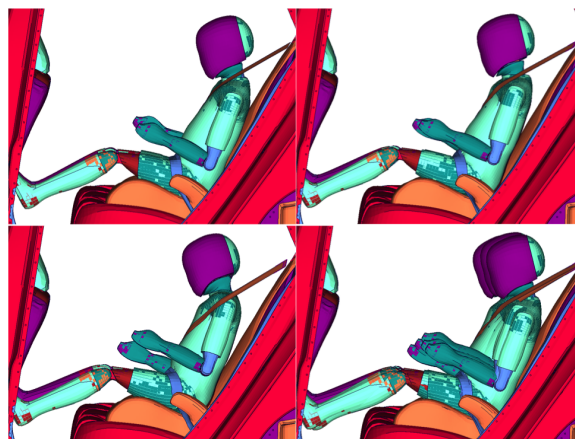

Figure 4.2.3: *Maximum forward displacement of Q6 model with manual pretensioner, TL: T0, TR:T1, BL: T2, BR: T0,T1 and T2.*
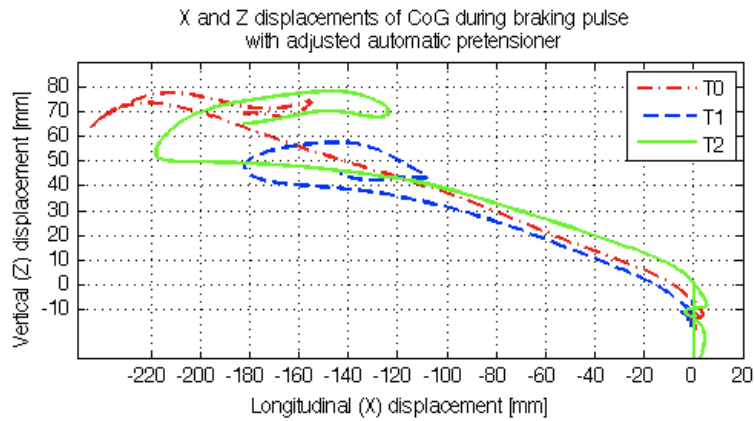
Figure 4.2.4: *X and Z displacement of CoG during braking test runs with automatic pretensioner*
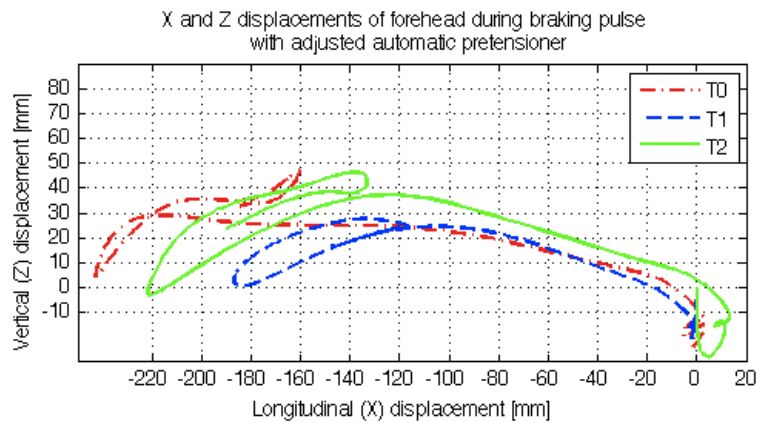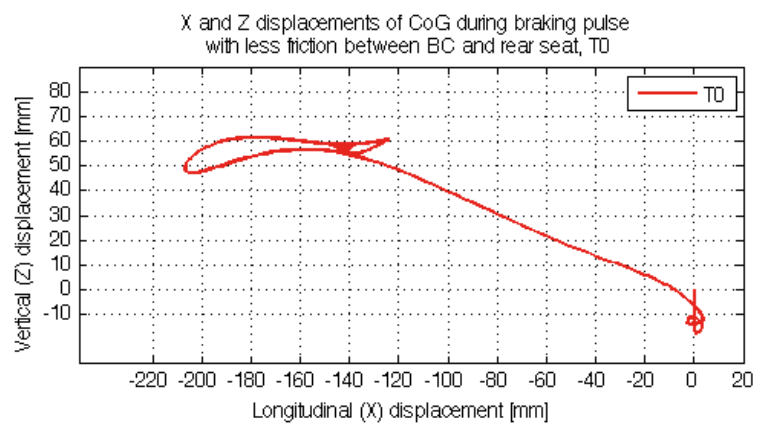

Figure 4.2.5: *X and Z displacement of forehead during braking test runs with automatic pretensioner*

Figure 4.2.6: *X and Z displacement for the head's CoG during braking for T0 with lower friction between BC and rear seat*
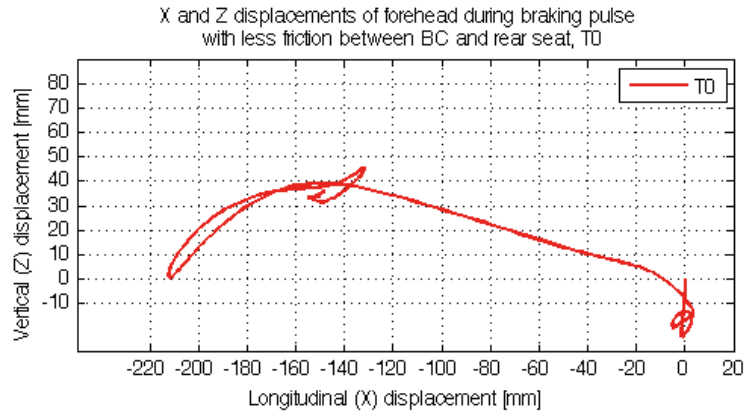
Figure 4.2.7: *X and Z displacement for the forehead during braking for T0 with lower friction between BC and rear seat*

4.2.3 Automatic and manual correlation

The tilting angles during the turning maneuvers with T0, both for the automatic and manual pretensioner, are seen in Figure 4.2.8 .The tilting angle during turning maneuver for automatic pretensioner was larger than for manual pretensioner. The head angle was measured between the mid point of the abdomen (N1, see Figure 3.2.14) to the midpoint of the forehead (N3). The same midpoint of the abdomen was used in measuring the tilting angle of the torso, the second point was chosen as the middle of the upper thorax (N2).
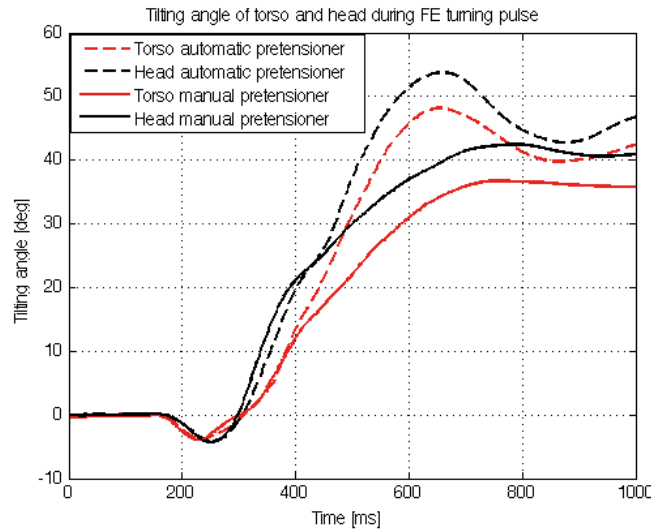
Figure 4.2.8: *Tilting angle of head and torso for both manual and automatic pretensioner*

In the FE simulations, for both the manual and automatic pretensioner, the X and Z displacements of the head's CoG were greater than the Q6 ATD's displacements. Furthermore, the Q6 model's forehead trajectory displays a forward movement starting with a positive vertical movement and finishing with a negative vertical movement. In comparison the head's CoG trajectory only displays forward movement combined with a positive vertical movements (Figure 4.2.1, Figure 4.2.2, Figure 4.2.4 and Figure 4.2.5). In Table 4.2.1 the maximum forward displacement for the simulations with the manual (TR-FE 1-3) pretensioner for T0, T1 and T2 is compared to the automatic (TR-FE 5-8) pretensioner and the simulation with low friction (TR-FE 9).

In Table 4.2.2 the correlation between the tilting angles T1 and T2 and the distance traveled along the curve during FE-turning maneuver is shown. The Q6-model only traveled 2.5-3.4m along the curve prior to reaching the tilting angles of T1 and T2. This corresponds to the vehicle traveling only 0.2-0.4 m in the Y direction along the track. NB! The tilting angles in Table 4.2.2 are extracted from the turning maneuver as

Table 4.2.1: Maximum longitudinal displacements of the forehead and CoG during braking pulse. Lateral tilting angles prior to braking at simulation time 300ms

Test Runs	Max Displacement Forehead [mm]	Max Displacement Head CoG [mm]	Tilting angle prior to braking at time = 300ms [deg]
TR-FE 1	210	211	0
TR-FE 2	218	222	5.7
TR-FE 3	220	223	15
TR-FE 5	231	232	0
TR-FE 6	187	182	5.8
TR-FE 7	221	218	13
TR-FE 9	212	208	0

close as possible as the tilting angles shown in Table 4.2.1. The time step used in the simulation did not allow a more exact extraction.

Table 4.2.2: The FE-vehicles position relative to the Q6 FE-models tilting angles during the the turning maneuver.

Tilt angle [deg]	Distance traveled [m]	X translation [m]	Y translation [m]
5.9	2.5	2.49	0.2
13.3	3.2	3.17	0.36
15	3.4	3.37	0.41

4.3 Comparison between FE-simulation and physical testing

The physical vehicle had traveled further along the turning curve than the FE-model had when achieving the same tilting angles, see Table 4.2.2 and Table 4.1.2. The lateral accelerations for the physical vehicle had an average of 7.8 m/s^2 whereas the FE-simulation had 13.8 m/s^2, see Table 4.3.1. The longitudinal velocity during the turning event was greater for FE simulations (50 km/h) in comparison to the physical test average (43km/h). During the braking maneuvers, the initial velocity prior to braking was 70km/h for the FE-simulation and an average of 67km/h for the physical tests. Further, both the physical tests and the FE simulations had the same average decelerations for braking maneuver, see Table 4.3.1. The forward displacements of the forehead and

Table 4.3.1: Differences in acceleration and velocity between Physical testing and FE-simulation.

Maneuver	Velocity/Acceleration	Physical testing	FE-simulation
Turn	Velocity [km/h]	43	50
Turn	Lateral acceleration [m/s^2]	7.8	13.8
Brake	Initial velocity [km/h]	67	70
Brake	Deceleration [m/s^2]	8.4	8.4

the head's CoG for the physical testing was compared to the FE-simulations using the manual pretensioner, see Table 4.3.2. The displacements from the FE-simulations were greater than for the physical tests for both the forehead and the head's CoG. The respective tilting angles of T0, T1 and T2 for the physical testing and FE-simulations are seen in Table 4.1.1 and Table 4.2.1.

In Figure 4.3.1 the X and Z displacements of the FE simulation with manual pretensioner are shown together with the physical average value of the braking maneuvers. The left column of figures present the head's CoG displacements for T0, T1 and T2 and the right column presents the forehead's displacements. In both CoG and forehead displacements the physical testing results have lower X and Z displacement values than what the FE-simulations indicate (Figure 4.3.1).

Table 4.3.2: Average values of the forward displacements the physical testing compared to the FE-simulations when manual pretensioner was used.

Tilt	Avg Max Displacement Forehead Physical [mm]	Max Displacement Forehead FE-manual [mm]	Avg Max Displacement Head CoG Physical [mm]	Max Displacement Head CoG FE-manual [mm]
Brake T0	115	210	90	210
Brake T1	130	220	100	220
Brake T2	165	220	125	225
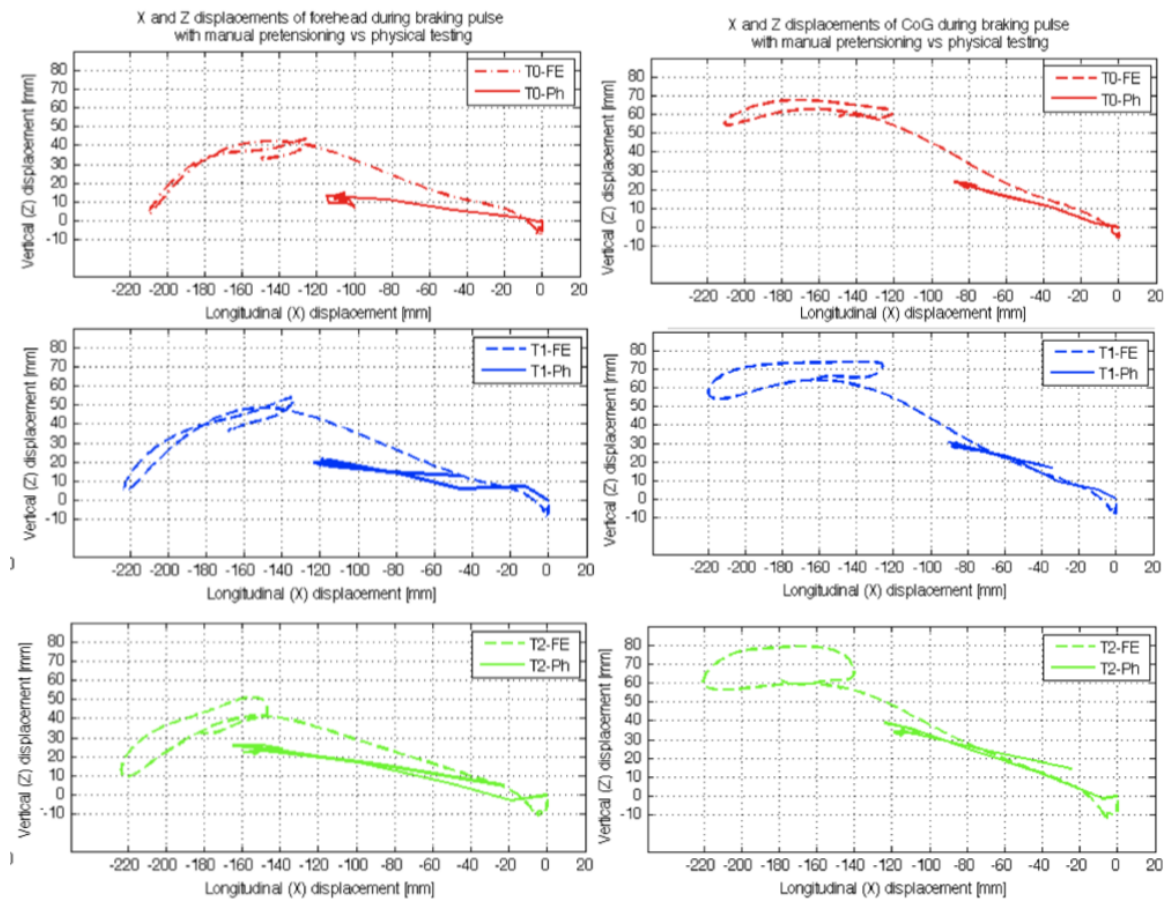
Figure 4.3.1: *To the left: X and Z displacements on the head's CoG depicting the FE-simulation with manual pretensioner vs physical testing data, from the top; T0, T1 T2. To the right: X and Z displacements on the forehead depicting the FE-simulation with manual pretensioner vs physical testing data, from the top; T0, T1 T2.*

25

5 Discussion

There are several issues needed to be considered when comparing physical data to FE-simulations. This chapter presents the major issues concerning the different method steps as well as discussions about the correlation between the physical testing and FE simulation results.

5.1 Differences in initial test set-up

There were a few major differences regarding the test set-ups of the physical testing and the FE-simulation. As mentioned in Table 3.0.1 the physical vehicle was a Volvo XC70 and the FE-vehicle model was a Volvo V60. This created a difference in the position of the upper webbing guiding loop, which impacts the angle at which the shoulder belt is positioned across the torso. In addition the Q6 ATD was positioned on a Britax Kid Plus BC whereas the Q6 model was placed on an in-house BC model, see Figure 3.0.1. Their initial geometrical difference did also affect the shoulder belt angle.

Another evident difference was the seating position within the vehicle, where the Q6 ATD was placed in the right side of the rear seat and the Q6 model was placed in the left side of the rear seat, mainly due to initial modeling advantages. This does not affect the results other than by having to take positive/negative lateral coordinates and directions into account. In accordance, the pulse set-up for the turning event was made to turn left, in contrast to the right turn during the physical testing to get an inboard motion of the occupant, Figure 3.1.2. The FE-simulated vehicle was also set to have a turning radius of 14m, but this was measured from the vehicle's longitudinal centerline, rather than ∼1m outside the vehicle as was the case with the physical turning test. The longitudinal speed was 50km/h during the FE-simulation and the average speed during the physical turning maneuvers was 43 km/h. This combined with a smaller radius for the FE-simulations made the lateral acceleration greater during the FE-simulation. The driver's instruction was to drive with a constant speed of 50 km/h during the physical testing.

One advantage with FE-simulations compared to physical testing is their total repeatability. However, during this study the experienced test driver managed to perform test runs with good repeatability which can be seen in Figure 3.2.4. The linearized brake pulse which was based on the physical test runs can therefore be considered sufficient.

5.2 Physical tests

When analyzing the forehead and head's CoG displacement results from the physical tests, Figure 4.1.1 and Figure 4.1.2, the starting positions of each run were set to (X,Z)=(0,0). However, the results also showed that the end positions varied between each run, even though the end position was extracted from when the head returned to rest on the headrest, and therefore in theory should have been the same. The rotation of the head may differ and therefore cause this slight difference in final coordinates. In addition, the camera frames were sampled with 80 ms intervals which may cause the exact time step at which the head touched the headrest to be missing.

The physical testing showed that the Q6 ATD experienced a maximum tilting angle of 15° during the turning maneuvers.The estimated initial angles for braking at T1 and T2 were ∼ 6° and ∼ 12° which in fact are lower than what the turning maneuver showed. The results show that a higher initial tilting angle contributes to a larger forward displacement of the forehead and head's CoG, Figures 4.1.2 and 4.1.1. An initial tilting angle of 15° was never tested during the physical braking maneuvers but the results suggests that the forward displacement of the forehead and head's CoG during such a braking maneuver should have been even greater than for T1 and T2. The accelerations, both lateral and longitudinal, are of the magnitude that could be experienced during normal driving scenarios when for example speeding through a roundabout or on a highway exit ramp followed by a stop sign. In these scenarios a child would experience lateral accelerations followed by longitudinal deceleration such as the physical test set-up simulates. As the results show that larger tilting angles result in larger forward displacements one could argue that even normal driving conditions causing lateral accelerations could increase the risk of head impact when performed in a turning-braking sequence. This also implies that children who tend to lean in towards the middle to get a better forward view of the road (Jakobsson et al., 2011a) risk having a larger forward displacement of the head during a braking scenario than those who sit in an upright position.

When comparing the T0, T1 and T2 tilting angles the difference in forward displacement of T0 and T1 was smaller than the difference between T1 and T2. As the tilting angle increased, the shoulder belt had less and less effect in restraining the occupant's torso. An increasing forward displacement due to the belt being positioned further out on the shoulder was also seen in a study by Stockman et al. (2012). During the T1 braking, the shoulder belt was still in interaction with the shoulder area which may explain this small difference between T0 and T1. During the T2 braking the shoulder belt had slipped off which would explain the larger difference in forward displacement between T1 and T2.

5.3 FE-simulation

The tilting angles after turning with the Q6 model were greater than for the physical results. This can be an effect from driving with a slightly higher velocity; 50km/h compared to the physical test where the average velocity was 43 km/h. This in combination with previously mentioned smaller curve radius led to higher lateral accelerations. Just as for the physical tests the FE results show that if the maximum tilting angle from the turning simulations would have been used in a braking scenario, the forward displacements would have become greater. The risk of impacting the front seat with the forehead would then increase.

When analyzing the FE simulation it was clear that how well the pretensioner tightened the seat belt played an important role in the seat belt position prior to braking, compare Figures 3.2.10 and Figure 3.2.13. When pre-tensioning the belt manually, the amount of slack between T0, T1 and T2 was similar by visual judgement. The results from the manual pre-tensioning also indicated that a larger tilting angle resulted in a larger forward displacement, which is in agreement with the results from the physical tests.

5.3.1 Seat Belt

A manual pre-tensioning of the seat belt by using boundary prescribed motion with adjustments resulted in a tighter fit prior to braking than with the automatic pretensioner. The negative aspect of this method is that the model and simulation needs to be prepared in two steps as described in Section 3.2.4. This could become tiresome for future simulations as the complexity of a model increases and the number of models to be simulated increase.

When placing the shoulder belt, which would be pre-tensioned with the automatic pretensioner, the number of 2D elements was extended to pass below the guiding loops and slightly turn towards the buckle in order to create a tight fit. This resulted in some slack in the lower region of the shoulder belt after the pre-tensioning phase and prior to the braking and turning maneuvers. One could argue that using 1D beam elements for the belt in this region would have allowed for a smoother pre-tensioning of the belt. However, the 2D elements were needed in order to keep the lower part of the shoulder belt in a correct position under the guiding loops after the pre-tensioning phase. It is also of great significance that the 1D elements never approach the Q6 model since it may cause penetration issues and thereby a non-realistic belt geometry. During automatic pre-tensioning the 1D beam elements also penetrated the inner part of the BC's guiding loops, see Figure 3.2.9, even though zero-beam elements were added. This caused the 2D elements of the shoulder belt to have a final position prior to braking placed close to the abdomen and therefore not be in contact with the BC. This was decided to be of a greater disadvantage for the results than if all slack would have been eliminated in this area. This slack is most likely the reason for the larger maximum tilting angle during the turning pulse, see Figure 4.2.8, than when using the manual pretensioner. There was a trade-off between the amount of 1D elements vs. 2D elements in the lower region of the shoulder belt and the final result indicates that this possibility needs to be worked with further.

The overall evaluation of pre-tensioning the belt during FE-simulations comes down to long-term usability. If the automatic pretensioner were further fine tuned with reliable and tight-fitting belts as a result, it would definitely be the optimal solution mainly due to the fact that the whole simulation could be done in one sweep. However, the results of this thesis indicate that the manual pretensioner gives a tighter fit and should therefore be used.

5.3.2 Braking vs. crashtest

There are several simulation issues specific to the low pulse scenario created for this thesis that need to be taken into account. As the Q6 model is not immediately subjected to a large forward acceleration, which normally is the case when simulating a crash, the Q6 model has time to settle in its seat due to gravity. This

is a problem that arises even though the Q6 model has been pressed into the BC and the BC itself into the rear seat prior to simulation. Pressing the model further into the rear seat bottom and seat back would not have eliminated this issue if not the Q6 model had been pre-simulated in order to allow its internal parts to settle due to gravity. The fact that gravity has time to impact the model creates a problem since the belt has been placed and manually adjusted for the initial position of the Q6 model. As it moves in a negative Z direction and positive X direction seat belt slack is created. In the event of a crash, both in the physical world and when simulating, the belt pretensioner used would eliminate that slack. The force applied by the original pretensioner however was far too severe, as it was designed for crash scenarios and here only should be used as a belt positioner and gentle slack remover. The objective for the pretensioner in this simulation was not to prohibit forward displacement of the Q6 model as the accelerations are not severe.

When using the braking pulse created based on the physical test runs, the Q6 model initially transfers rearward in the vehicle as it settles due to gravity, which is why the rear seat back needed to be taken into account. As the simulations performed in this thesis also included turning, causing the Q6 model to tip over towards the center of the vehicle, the center seat also needed to be in place in order to achieve reliable results. Every part added to the simulation model will result in a more complex model, causing more contacts definitions needed.

5.4   FE-simulations vs. physical tests

The upper body of the Q6 model, including torso and head, does not only tilt inwards as a rigid body but bends during the turning maneuver. This result is supported by observing the difference of head and torso tilting angles seen in Figure 4.2.8. An analysis of the results from the physical testing shows that the Q6 ATD tilts rather than bends which indicates that the Q6 model in fact is more flexible than the Q6 ATD. The strict tilting behavior is also noticed in children of similar stature (Bohman et al., 2011b). The bending behavior of the torso was not taken into account when positioning the Q6 model during the braking pulse simulations as this was a result that was observed too late. The impact this could have had on forward displacement of the head has not been investigated. Future work could take this into account by creating one long maneuver pulse starting with a turning maneuver and finishing with a brake maneuver. It is also important to note that there exists another Q6 model which is validated for high pulse side impacts and the Q6 model used in this thesis is validated for high pulse frontal impacts. This may also have an effect on the bending behavior.

The correlation between the FE-simulation and the physical testing, Section 4.3, show that in order to reach tilting angles of 5-11° the distance traveled along the FE-turning curve only ranges from ∼4-7m. This corresponds to a y-translation of the vehicle of only 0.4-1.2m and indicates that the vehicle does not need to be subjected to a large lateral displacement in order for the occupant to tilt to the angles which result in a larger forward displacement. In order to reach the greater tilting angles of 13.3° and 15° the results show that a much greater y-translation is needed. When analyzing the images from the physical testing one can observe that the Q6 ATD rests its lower arm on the BCs guiding loops when approaching ∼12° which might be the reason why the tilting rate stagnated. The tilting movement then continues up to 15° due to the fact that the BC itself is starting to tilt. If the Q6 ATD's arms been rotated up for the initial seating position the Q6 ATD would most likely have continued with a greater tilting rate to a greater angle and definitely would have reached 15° faster than what was observed in this study.

When analyzing the forward displacement of the BC during the braking maneuver it was identified that the movement was greater than the movement identified during the physical testing. In order to mitigate this problem the friction between the BC and rear seat was increased as described in Appendix B. This caused the Q6 model to slide forward on top of the BC rather than moving together with it which was more similar to the physical testing. During the FE simulation turning maneuver the BC's tilting movement also differs in comparison to the corresponding physical tests. The BC tends to tilt upward together with the Q6 model to a greater extent than seen during the physical testing.

A previous study conducted by Stockman et al. (2012) studied the forward displacement of the forehead of child volunteers during a low pulse braking scenario similar to the one tested in this thesis. The kinematics of the children resemble the movement of the Q6 model to a greater extent than the movement of the Q6 ATD. The children of similar stature as the Q6 model and Q6 ATD had forward displacements between 200-300mm whereas the Q6 ATD only reached about 120mm and the Q6 model reached about 220mm. When analyzing the forward translational movement of the entire Q6 (both ATD and model), the Q6 model showed a greater forward displacement along the BC than what could be seen for the Q6 ATD. This also contributes to the fact

that the forward displacement of the forehead was greater for the Q6 model than for the Q6 ATD.

When observing the X and Z displacements of the head, the combination of the forehead and the head's CoG displacements indicate that a rotational movement of the head occurs during the FE simulations. The trajectories of the forehead and head's CoG during the physical tests show almost a linear movement indicating a stiffer neck with no rotational movements, see Section 4.3. The children in the study by Stockman et al. (2012) also showed indications of a rotational movement of the head similar to the rotational movement observed in the FE-model simulations.

One of the main injury mechanisms in forward collisions of forward facing children is identified as hitting the head in the front seat back (Bohman et al., 2011a), however, no validation to real children was performed in this thesis. The risk of hitting the head in the front seat back can increase with larger forward displacement of the head and therefore this thesis gives input to the understanding of such potential events. How this behavior translates onto a crash pulse has not been thoroughly investigated and therefore, no conclusions can be drawn.

6   Conclusions

Using the Q6 ATD and Q6 model in low pulse maneuvers is technically possible even though some adjustments have to be made to the original models. It is also important to keep in mind that both the Q6 ATD and Q6 model are designed for high pulse crash scenarios and are therefore not validated for low pulse maneuvers. The following paragraphs discuss each of the research questions stated in Section 1.2.

The kinematic trends observed in the forward displacement of the head are similar when comparing the Q6 model with the manual pretensioner and the Q6 ATD. Both the Q6 model and Q6 ATD show that a larger torso tilting angle results in a larger forward displacement. This thesis shows indications of the Q6 model being more flexible in the neck structure than the Q6 ATD.

Both the physical tests and FE simulations of the turning maneuver show that the Q6 tilts inward the vehicle causing it to slip out of its shoulder belt. This, in combination with a braking maneuver including a tilted Q6, show that the forward displacement of the head is larger than if the Q6 was seated in an upright position. The risk of hitting the head in the front seat back can increase with larger forward displacement of the head and therefore this thesis gives input to the understanding of such potential events. How this behavior translates onto a crash pulse has not been thoroughly investigated and therefore, no conclusions can be drawn.

In pre-crash scenarios when turning occurs before braking, it is concluded that both the Q6 ATD's and the Q6 model's head has a greater longitudinal displacement with increasing tilting angle. This indicates that a combination of pre-crash maneuvers may increase the risk of impacting the head as described above.

7 Recommendations for further research

The area of pre-crash simulations of ATDs is relatively new and not many studies have been made on the matter. In order to fully understand the possibilities of using FE-models for simulation of low pulse maneuvers, a validation of the Q6 ATD and the Q6 model at these pulses needs to be carried out in comparison to real children. A more extensive study comprising children of different ages as well as variations of the test maneuvers would greatly benefit this research field. A standardization of test-set up for low pulse maneuvers would also be beneficial for further research.

In order to create a more refined model for low pulse simulation the authors recommend that the automatic pretensioner used in this thesis is further tuned to remove slack in a more proficient manner. Further studies on the effects of a pre-crash maneuver taking place prior to crash are needed to analyze how a braking and/or turning maneuver effects the outcome of the crash.

References

Arbogast, K. B. et al. (2009). "Effectiveness of belt positioning booster seats: an updated assessment". In: *Pediatrics* 124.5, pp. 1281–6. DOI: 10.1542/peds.2009-0908.

Automotive Handbook (2011). Vol. 8th Edition. 978-1-119-97556-4. Postfach 11 29, D-73201 Plochingen: Robert Bosch GmbH.

Bidez, M. W. et al. (Apr. 2005). "Small Occupant Dynamics in the Rear Seat: Influence of Impact Angle and Belt Restraint Design". In: Copyright © 2005 SAE International. DOI: 10.4271/2005-01-1708. URL: http://dx.doi.org/10.4271/2005-01-1708.

Bohman, K. et al. (Feb. 2011a). "Head injury causation scenarios for belted, rear-seated children in frontal impacts". In: *Traffic Injury Prevention* 12.1, pp. 62–70. DOI: 10.1080/15389588.2010.526159.

Bohman, K. et al. (2011b). "Kinematics and shoulder belt position of child rear seat passengers during vehicle maneuvers". In: *Annals of Advanves in Automotive Medicine* 55, pp. 15–26.

Bose, D. et al. (Oct. 2008). "Influence of active muscle contribution on the injury response of restrained car occupants". In: *Ann Adv Automot Med* 52, pp. 61–72.

Burdi, A. R. et al. (1969). "Infants and children in the adult world of automobile safety design: Pediatric and anatomical considerations for design of child restraints". In: *Journal of Biomechanics* 2.3, pp. 267 –280. ISSN: 0021-9290. DOI: 10.1016/0021-9290(69)90083-9. URL: http://www.sciencedirect.com/science/article/pii/0021929069900839.

Copes, W. S. et al. (Oct. 1989). "Progress in Characterizing Anatomic Injury". In: 33rd Annual Proceedings, October 2-4.

DeSantis, K. K. et al. (Nov. 1994). "Survey of Older Children in Automotive Restraints". In: DOI: 10.4271/942222. URL: http://dx.doi.org/10.4271/942222.

Durbin, D. R. et al. (2003). "Belt-positioning booster seats and reduction in risk of injury among children in vehicle crashes". In: *JAMA* 289.21, pp. 2835–40. DOI: 10.1001/jama.289.21.2835.

Durbin, D. R. et al. (2005). "Effects of Seating Position and Appropriate Restraint Use on the Risk of Injury to Children in Motor Vehicle Crashes". In: *Pediatrics* 115.3, e305–e309. DOI: 10.1542/peds.2004-1522. eprint: http://pediatrics.aappublications.org/content/115/3/e305.full.pdf+html. URL: http://pediatrics.aappublications.org/content/115/3/e305.abstract.

EuroNCAP (2012). URL: http://se.euroncap.com/se/tests.aspx.

Hallquist, J. (2007). *LS-DYNA Keyword User's Manual*. 0-9778540-2-7. Livermore Software Technology Corporation (LSTC).

Hammarström, J. et al. (2011). *Comparison study of the two pediatric aids: Hybride III 6-year-old and Q6*. Bachelor's thesis. Halmstad university.

Humanetics (2010). *Humanetics Innovative Solutions*. URL: http://www.humaneticsatd.com/crash-test-dummies/children.

Jakobsson, L. et al. (2005). "Safety for the growing child - Experiences from Swedish accident data". In: *ESV* 05-0330. URL: http://www-nrd.nhtsa.dot.gov/pdf/esv/esv19/05-0330-O.pdf.

Jakobsson, L. et al. (2011a). "Older Children's Sitting Postures when Riding in the Rear Seat". In: IRC-11-44.

Jakobsson, L. et al. (2011b). "Rest Seat Safety in Frontal to Side Impacts - Focusing on Occupants from 3YRS to Small Adults". In: *ESV* 11-0257. URL: http://www-nrd.nhtsa.dot.gov/pdf/esv/esv22/22ESV-000257.pdf.

Johansson, M et al. *Child safety in vehicles: validation of a mathematical model and development of restraint system design guidelines for 3-year-olds through mathematical simulations*. URL: http://www.ncbi.nlm.nih.gov/pubmed/19746311.

Johansson, M. (2008). "Child Safety in Car Crashes". PhD thesis. Göteborg: Department of Applied Mechanics.

Lehmann, I. (2012). "Q dummy modeling". In: vol. COVER / CASPER and EPOCH FINAL WORKSHOP. CASPER - Child Advanced Safety Project for European Roads. Berlin, Germany. URL: http://www.biomechanics-coordination.eu/downloadables/Child%20Safety%20Final%20Workshop%2013-15%20March%202012/22_Overview%20of%20CASPER%20dummy%20models-Lehmann.pdf.

Lubbe, N. (2010). "Comparison of Hybrid III 6yo and Q6 child dummies in high severity frontal impact tests". In: vol. 8th International Conference. TuV Sud Akademie GmbH. Munich, Germany: Protection of Children in Cars.

Maurath, C. A. (2008). *Development and validation of a finite element model of the Q3 anthropomorphic testing device*. Tech. rep. URL: http://search.proquest.com/docview/89126830?accountid=10041.

Morris, R. et al. (June 2005). "Improved Understanding of Passenger Behaviour During Pre-Impact Events To Aid Smart Restraint Development". In: 05-0320. URL: http://www-nrd.nhtsa.dot.gov/pdf/esv/esv19/05-0320-O.pdf.

Näringsdepartementet (2004). *Fortsatt arbete för en säker vägtrafik*. Proposition. URL: http://www.regeringen.se/sb/d/108/a/24237.

NCHS (2012a). *10 Leading Causes of Injury Deaths by Age Group - Highlighting Unintentional Injury Deaths, United States 2009*. Datasheet. National Center for Health Statistics (NCHS). URL: http://www.cdc.gov/Injury/wisqars/pdf/10LCD-Age-Grp-US-2009-a.pdf.

— (2012b). *10 Leading Causes of Injury Deaths by Age Group - Highlighting Violence-Related Injury Deaths, United States 2009*. Datasheet. National Center for Health Statistics (NCHS). URL: http://www.cdc.gov/Injury/wisqars/pdf/Leading_Causes_Injury_Deaths_Age_Group_Highlighting_Violence-Related\%20Injury_Deaths_US_2009-a.pdf.

Ottosen, N. et al. (1992). "Introduction to the FINITE ELEMENT METHOD". In:

Peden, M. et al. (2008). *World report on child injury prevention*. Tech. rep. World Health Organisation. URL: http://www.who.int/violence_injury_prevention/child/injury/world_report/report/en/index.html.

Scheidler, M. G. et al. (Nov. 2000). "Risk factors and predictors of mortality in children after ejection from motor vehicle crashes". In: *J Trauma* 49.5, pp. 864–8.

Scullion, P. et al. (Apr. 2009). "Injury Mechanism of the Head and Face of Children in Side Impacts". In: DOI: 10.4271/2009-01-1434. URL: http://dx.doi.org/10.4271/2009-01-1434.

Sethi, D. et al. (2008). *European report on child injury prevention*. Tech. rep. ISBN 978 92 890 4295 6. WHO Regional Office for Europe. URL: http://www.euro.who.int/en/what-we-do/health-topics/Life-stages/child-and-adolescent-health/publications/2011/european-report-on-child-injury-prevention.

Stockman, I. et al. (2012). "Kinematics of Child Volunteers and Child Anthropomorphic Test Devices during Emergency Braking Events in Real Car Environment". In: *Traffic Injury Prevention*. DOI: 10.1080/15389588.2012.688151. eprint: http://www.tandfonline.com/doi/pdf/10.1080/15389588.2012.688151. URL: http://www.tandfonline.com/doi/abs/10.1080/15389588.2012.688151.

Trafikverket (2012). *SÄKER TRAFIK Säker Trafik - Nollvisionen på väg*. 781 89 Borlänge. URL: http://publikationswebbutik.vv.se/upload/6562/100503_saker_trafik_nollvisionen_pa_vag.pdf.

Wernicke, P. et al. (2011). "Experiences with older children (Q6) in hardware and simulations". In: vol. 9th International Conference. TuV Sud Akademie GmbH. Munich, Germany: Protection of Children in Cars.

Wismans, J. et al. (Apr. 2008). *Q-dummies Report Advanced child Dummies and Injury Criteria for Frontal Impact*. Tech. rep. 514. URL: http://eevc.org/publicdocs/EEVC_WG12&18_DOC514_Q-dummies_&_Criteria-April_2008.pdf.

List of Tables

List of Figures

A Q6 Physical ATD

In Table A.0.1 and Table A.0.2 the masses and dimensions of the Q6 ATD are presented.

Table A.0.1: Mass of the Q6 ATD's different body parts (Hammarström et al., 2011).

Body part	mass [kg]
Neck+Head	3.94
Torso	9.57
Lower extremities	6.90
Upper extremities	2.49
TOTAL	22.90

Table A.0.2: Dimensions of the Q6 ATD's different body parts (Hammarström et al., 2011).

Body part	Dimension [mm]
Stature	1143
Sitting height	601
shoulder hight	362
Chest depth	141
Shoulder width	305
Hip width	223
Bum to knee	366

A.1 Physical Test Results

In Table A.1.1 the maximum values of the forward displacements and tilting angles for the physical testing are displayed. Throughout the report, the values have been rounded-off to the closest 5 and 0.5 values.

Table A.1.1: Longitudinal displacements and lateral tilting angles

Test Runs Physical	Max Displacement Forehead [mm]	Max Displacement Head CoG [mm]	Max Tilting Angle [deg]	Initial Tilting Angle [deg]
TR-Ph 1	127	95	-	0
TR-Ph 2	106	88	-	0
TR-Ph 3	-	-	14	0
TR-Ph 4	-	-	15	0
TR-Ph 5	130	99	7	7
TR-Ph 6	135	96	6	6
TR-Ph 7	162	133	11	11
TR-Ph 8	168	115	12	12

A.2 BC comparison

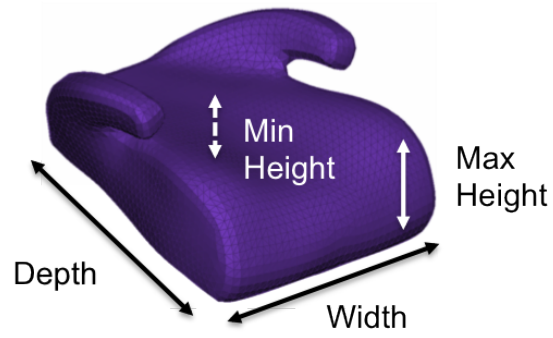Differences in physical and FE model dimensions of the BC, see Table A.2.1

Figure A.2.1: *Definitions of measurements of the booster cushion.*

Table A.2.1: Dimensions of the physical BC and the virtual BC.

Dimension	Physical	Virtual]
Width [cm]	41	37
Depth [cm]	36	36
Max height [cm]	13	12
Lowest height [cm]	9.5	8.8

B   LS-Dyna include files

A contact automatic general id was used for the zero beams element to have a edge2edge contact with 2mm. A contact automatic single surface id excluding zero beam elements, seat belt beams, Q6 model (Due to internal contacts) and 2D belt parts. For the exempted parts as well as some rear seat parts a contact automatic single surface was used. This contact was added to not cause penetrating issues between these parts.

In the original define friction file the friction was set to 0.5 between Q6 bum and BC, Q6 back and backrest (both the backrest behind the model as well as the middle seat) and between the BC and rear seat. For the shoulder and lap belt to the Q6 suit the friction was set to 0.3.To avoid sliding of the BC the friction was increased to 0.8 between BC and rear set. In crash simulations the friction between the Q6 suit and the BC was lowered to 0.3.

Some include files that were altered for this thesis were:

- *CONTACT_AUTOMATIC_GENERAL_ID

    Null beams for edgetoedge contact with 2mm. Contact file for zero beams elements added on the BC and the lower parts of the seat belt.

- *CONTACT_AUTOMATIC_SINGLE_SURFACE_ID

    SSTYP =6 excluding defined parts and creating contacts for everything else, FS=-2, using friction as described in the *DEFINE_FRICTION.

- *CONTACT_AUTOMATIC_SINGLE_SURFACE_ID

    SSTYP=2, creating contacts with defined parts. FS=-2 using friction as described in the *DEFINE_FRICTION.

- *DEFINE_FRICTION

    friction was set as described above.

- *CONTROLE_TIMESTEP

    The timestep was set to -0.7E-3ms.

- CONTROLE_TERMINATION

    The used termination times were; 100ms, 1000ms, 1560ms and 2950ms was used.